N70-27964

NASA TECHNICAL MEMORANDUM

NASA TM X-2023

NASA TM X-2023

CASE FILE COPY

PERFORMANCE OF AN AERODYNAMICALLY POSITIONED AUXILIARY INLET EJECTOR NOZZLE AT MACH NUMBERS FROM 0 TO 2.0

by Donald L. Bresnahan

Lewis Research Center
Cleveland, Ohio 44135

NATIONAL AERONAUTICS AND SPACE ADMINISTRATION • WASHINGTON, D. C. • MAY 1970

1. Report No.	2. Government Accession No.	3. Recipient's Catalog No.
NASA TM X-2023		

4. Title and Subtitle	5. Report Date
PERFORMANCE OF AN AERODYNAMICALLY POSITIONED AUXILIARY INLET EJECTOR NOZZLE AT MACH NUMBERS FROM 0 TO 2.0	May 1970
	6. Performing Organization Code
7. Author(s) Donald L. Bresnahan	8. Performing Organization Report No. E-5536
9. Performing Organization Name and Address Lewis Research Center National Aeronautics and Space Administration Cleveland, Ohio 44135	10. Work Unit No. 720-03
	11. Contract or Grant No.
	13. Type of Report and Period Covered Technical Memorandum
12. Sponsoring Agency Name and Address National Aeronautics and Space Administration Washington, D.C. 20546	14. Sponsoring Agency Code

15. Supplementary Notes

16. Abstract

An 8.5-inch (21.59-cm) model was used with aerodynamically positioned tertiary inlet doors and secondary flaps. The flaps and doors were stable at all power settings and free-stream Mach numbers. Nozzle efficiencies of 0.98 were obtained at takeoff with a nozzle pressure ratio near 3.0, and 0.971 at Mach 2.0 with a nozzle pressure ratio near the design value of 29.0. At subsonic cruise both the nozzle performance and the floating flap position was sensitive to nozzle pressure ratio. For example, at Mach 0.9 increasing pressure ratio from 3.27 to 4.20 increased nozzle efficiency from 0.868 to 0.888 and reduced the nozzle area ratio from 2.93 to 2.38.

17. Key Words (Suggested by Author(s))	18. Distribution Statement
Aerodynamically positioned Nozzle Auxiliary inlet ejector Propulsion Nozzle Performance	Unclassified - unlimited

19. Security Classif. (of this report)	20. Security Classif. (of this page)	21. No. of Pages	22. Price*
Unclassified	Unclassified	49	$3.00

*For sale by the Clearinghouse for Federal Scientific and Technical Information
Springfield, Virginia 22151

PERFORMANCE OF AN AERODYNAMICALLY POSITIONED AUXILIARY INLET EJECTOR NOZZLE AT MACH NUMBERS FROM 0 TO 2.0

by Donald L. Bresnahan

Lewis Research Center

SUMMARY

An experimental investigation was conducted in the Lewis Research Center's 8- by 6-Foot Supersonic Wind Tunnel to determine the performance characteristics of a cold flow 8.5-inch (21.59-cm) diameter auxiliary inlet ejector with aerodynamically positioned tertiary inlet doors and secondary flaps. The design pressure ratio of the nozzle was 29.0. Two primary nozzles were tested: a small nozzle with a throat to nacelle area ratio of 0.185 to simulate operation at subsonic and supersonic cruise and nonafterburning acceleration, and a large nozzle with an area ratio of 0.261 to simulate afterburning takeoff and acceleration and also idle descent.

The flaps (which could reduce the exit area by 38 percent) and the inlet doors were stable at all power settings and free-stream Mach numbers. For a typical trajectory, the flaps were closed at takeoff and during subsonic acceleration. The flaps began to open at Mach 1.0 and were fully open at Mach numbers of 1.47 and above. The auxiliary inlets were full open at takeoff and partially open at subsonic cruise. During acceleration the inlets were closed at speeds above Mach 0.8.

Nozzle efficiencies of 0.98 were obtained at takeoff with a nozzle pressure ratio near 3.0 and 0.971 at Mach 2.0 with a nozzle pressure ratio of 27.6. At subsonic cruise both nozzle performance and floating flap position were sensitive to nozzle pressure ratio. For example, at Mach 0.90 increasing pressure ratio from 3.27 to 4.20 increased nozzle efficiency about 2 percent to 0.888 and reduced the nozzle area ratio from 2.93 to 2.38.

INTRODUCTION

The Lewis Research Center is evaluating various nozzle concepts appropriate for supersonic cruise applications. These nozzles must operate efficiently over a wide

range of flight conditions and engine power settings, necessitating extensive geometric variations. The performance of a low-angle plug nozzle and a variable-flap ejector nozzle designed for a supersonic cruise aircraft are reported in references 1 and 2, respectively. Another nozzle type of interest is the auxiliary inlet ejector. At the supersonic cruise point, this nozzle is similar to the variable-flap ejector. However, at takeoff and subsonic flight conditions, auxiliary inlets open to admit tertiary air to minimize primary flow overexpansion. This tertiary air fills part of the shroud, reducing the amount of exit-area variation required with an associated reduction in boattail area. Internal performance for an auxiliary inlet ejector nozzle with fixed geometry has been reported in reference 3. An ejector nozzle with free-floating doors and fixed shroud exit areas is reported in reference 4. However, experimental results on auxiliary inlet ejector nozzles with fully floating components are not generally available. The present investigation, therefore, was conducted to determine the performance of an aerodynamically positioned auxiliary inlet ejector nozzle over a range of free-stream Mach numbers from 0 to 2.0. Two primary nozzles were tested: a small nozzle to simulate a configuration for nonafterburning acceleration and for subsonic and supersonic cruise, and a large nozzle to simulate a configuration for afterburning takeoff and acceleration and for idle descent.

SYMBOLS

A	area
C_d	nozzle flow coefficient
D	drag
d	diameter
F	thrust
F_{ip}	ideal primary thrust based on measured primary flow
F_{is}	ideal secondary thrust based on measured secondary flow
$\frac{F - D}{F_{ip}}$	nozzle gross thrust coefficient
$\frac{F - D}{F_{ip} + F_{is}}$	nozzle efficiency
M	Mach number
P	total pressure
p	static pressure

r	radius
T	total temperature
W	weight flow rate
x	axial distance
y	radial distance in plane of primary total-pressure rake
α	external primary nozzle angle
β	boattail angle
τ	temperature ratio, T_s/T_p
ω	weight flow ratio, W_s/W_p

Subscripts:

i	ideal
max	maximum
p	primary
s	secondary
0	free-stream
7	nozzle inlet
8	nozzle throat
9	nozzle exit

APPARATUS AND INSTRUMENTATION

Installation in 8- by 6-Foot Supersonic Wind Tunnel

A schematic drawing of the model support system in the 8- by 6-Foot Supersonic Wind Tunnel showing the internal geometry and thrust-measuring system is shown in figure 1 with a photograph of the model installation in figure 2. The grounded portion of the model was supported from the tunnel ceiling by a vertical strut. The floating portion was supported by the primary and secondary air bottles cantilevered by flow tubes from external supply manifolds. The primary air bottle was guided by front and rear bearings. The secondary air passed through hollow crossover struts at station 100.66 to the annulus formed between the primary nozzle and the shroud. Since the primary and secondary flows enter the floating portion of the model support system normal to the force measurement axis, the entry momentum of the internal flows can be neglected in the cal-

culation of thrust. Therefore the load cell measured only the internal nozzle forces, the external pressure and viscous forces downstream of the skin break, and a tare force.

A static calibration of the thrust-measuring system was obtained by applying known forces to the nozzle and measuring the output of the load cell. A water-cooled jacket surrounded the load cell and maintained a constant temperature of 90° F (305.6 K) to eliminate errors in the calibration due to variations in temperature from aerodynamic heating.

The tertiary door and secondary flap positions were determined by measuring the angles from movies taken during the test runs.

Nozzle Configurations

Two basic variable nozzle configurations were tested, differing only in primary nozzle area. The small nozzle provided a throat to nacelle area ratio of 0.185 and simulated nonafterburning operation for subsonic acceleration and subsonic and supersonic cruise. The large nozzle had an area ratio of 0.261 and simulated afterburner-on operation for takeoff and transonic and supersonic acceleration and simulated low power operation for idle descent.

Each primary nozzle had 16 tabs that are used during reverse thrust operation. In practice the primary nozzle translates downstream to seal against the secondary nozzle and the primary leaves and tabs close to block the primary flow thereby directing it upstream through the tertiary doors. During forward thrust operation the tabs are in a position to provide some guidance to the flow expansion. An air guide is provided in the secondary annulus to direct some of the cooling flow over the leaves of the primary nozzle.

The ejector shroud had 16 single hinge auxiliary inlet doors on the 3° 23-minute fixed boattail portion of the model and 16 floating secondary flaps. The three doors at the 2, 6, and 10 o'clock locations were fixed in the closed position to simulate an installed condition within a wing structure, and the remaining 13 unsynchronized doors were free to float to admit tertiary air. The secondary flaps could reduce the exit area by 38 percent and were made up of leaves and seals which were free to float for the aerodynamic adjustment of exit area with pressure ratio. The juncture radius of the flaps was approximately 0.029 of the maximum model diameter. In figure 3 the flaps are shown in the open and closed positions. Figure 4 shows the auxiliary inlet area variation as a function of the tertiary door angle. With the 13 doors fully open, the auxiliary inlet area to small primary throat area ratio was 0.935.

Between the tertiary doors are hollow support beams which duct a portion of the secondary flow into the secondary flap cavity. This flow simulated that required for

film cooling of the shroud and exited through two internal annular slots on the flaps with exit areas that were 1.94 and 0.86 percent of the maximum model area. At low pressure ratios it was anticipated that this flow would pressurize this cavity to aid in closing the flaps. Basic nozzle dimensions, contour coordinates and static pressure instrumentation are shown in figures 5(a) to (h) and the variation of nozzle area ratio with boattail angle for the two primary throat areas is shown in figure 5(i).

In an effort to improve subsonic cruise performance, the small primary configuration was modified and retested at increased secondary flow rates in an attempt to force the flaps closed, thereby reducing the overexpansion losses. These modifications are shown in the following sketch.

(1) Plugged actuator link slots
(2) Plugged air guide holes previously open for door movement
(3) Door stops now on air guide
(4) Capability of fixing doors maximum open
(5) Capability of plugging air guide slot (all secondary flow through beams and secondary nozzle)

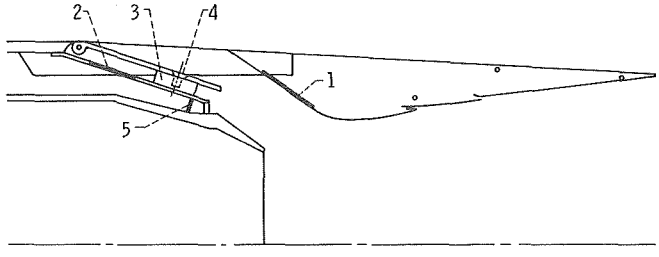

Configuration	Modifications
Nonafterburning 1	1, 2, and 3
Nonafterburning 2	1 to 4
Nonafterburning 3	1, 2, 3, and 5

Configuration 1 had the actuator link slots and the air guide holes plugged to prevent leakage and to direct more of the secondary flow through the beams into the secondary flap cavity where it could only exit through the annular cooling slots. If this higher flow rate increased the cavity pressure, it would tend to close the flaps. Configuration 2 was the same as configuration 1 but also had the tertiary doors fixed in the maximum open position. Configuration 3 was the same as configuration 1, but the air guide annulus was also plugged to force all the secondary flow through the beams and into the secondary flap cavity.

Nozzle Instrumentation

The model instrumentation is shown in parts of figure 5 and in figure 6(a). The primary and secondary total pressures were obtained by the use of total pressure probes as shown. The average primary total pressure was calculated from the integrated average pressure of each rake. Typical profiles are shown in figures 6(b) and (c).

Procedure

Nozzle performance was obtained over a range of pressure ratios and Mach numbers. The schedule shown in figure 7 was used as a guide for setting pressure ratio over the range of Mach numbers from 0 to 2.0 for each power setting. At each Mach number, data were taken at several nozzle pressure ratios near the values shown on the schedule. Since tunnel static pressure was fixed at a given Mach number, the nozzle pressure ratio was varied by changing the nozzle-inlet pressure. The maximum pressure ratio at each Mach number was restricted due to the limitations of the primary air supply. At each pressure ratio, corrected secondary weight flow ratio was varied up to a maximum of 0.06 of the primary flow for all power settings with the exception of idle descent where the corrected secondary weight flow ratio was set at approximately 0.14.

Data Reduction

Both primary and secondary flow rates were measured by means of standard ASME flowmetering orifices located in the external supply lines and the primary orifice was calibrated with an ASME nozzle of known discharge coefficient. Thrust-minus-drag measurements were obtained from a load cell readout of the axial forces acting on the floating portion of the model. Internal tare forces, determined by internal areas and measured pressures located as shown in figure 1, were accounted for in the thrust

calculation.

The only external friction drag charged to the nozzle was that downstream of station 136.90 shown in figure 1. That force acting on the portion of the nozzle between station 93.65 and 136.90 was also measured on the load cell, but was not considered to be part of the nozzle drag. Its magnitude was estimated using the semi-empirical flat-plate mean skin friction coefficient given in figure 6 of reference 5 as a function of free-stream Mach number and Reynolds number. The coefficient accounts for variations in boundary-layer thickness and profile with Reynolds number. Previous measurements of the boundary-layer characteristics at the aft end of this jet exit model in the 8- by 6-Foot Supersonic Wind Tunnel (fig. 5 in ref. 6), indicated that the profile and thickness were essentially the same as that computed for a flat plate of equal length. It also showed that the average momentum thickness to model diameter ratio was 0.019 for the range of Mach numbers investigated. The strut wake appeared to affect only a localized region near the top of the model and resulted in a slightly lower local free-stream velocity than measured on the side and bottom of the model. Therefore, the results of reference 5 were used without correction for three-dimensional flow effects or strut interference effects. The resulting correction was applied to the load-cell force.

The ideal gross thrust for each of the primary and secondary flows was calculated from the measured mass flow rate expanded from their measured total pressures to p_0 Provision was made to equate the ideal thrust of the secondary flow to zero if the total pressure was less than p_0. Nozzle efficiency is defined then as the ratio of the gross thrust-minus-drag to the ideal gross thrust of both primary and secondary flows:

$$\text{Nozzle efficiency} = \frac{F - D}{F_{ip} + F_{is}}$$

In addition, nozzle gross thrust coefficients, $(F - D)/F_{ip}$, are also presented.

RESULTS AND DISCUSSION

Nozzle Performance for Typical Flight Pressure Ratio Schedule

The auxiliary inlet ejector nozzle was tested with two primary nozzles to simulate afterburning and nonafterburning operation. Each configuration was tested over a range of nozzle pressure ratios and Mach numbers corresponding to a typical schedule for a supersonic turbojet engine (fig. 7). A summary of the performance characteristics over a range of free-stream Mach numbers at several simulated power settings is shown in figure 8. The corrected secondary weight flow ratio of 0.04 was selected as a basis for

comparison at all flight Mach numbers except at supersonic cruise where a flow ratio of 0.02 was selected.

The band of tunnel interference shown in the figures was a result of the terminal shock movement over the model. In free flight the flow field near the front of an ogive cylinder creates a terminal shock that moves aft rapidly with increasing flight speed and disappears downstream at speeds slightly above Mach 1. In a tunnel installation, however, large models retard the aft movement of the terminal shock. Therefore, the resultant boattail pressure drag can be influenced by tunnel installation effects particularly at speeds where the terminal shock is near the boattail. A more detailed discussion of this phenomenon is covered in reference 7.

At takeoff conditions it can be seen in figure 8(a) that high efficiencies of 0.980 and 0.982 were obtained with the large and small primary nozzles, respectively. In figures 8(b) and (c) it can be seen that the flaps were fully closed at this condition and the doors were fully open. As indicated in figure 8(d) secondary flow pumping was marginal at afterburning conditions since a secondary pressure equal to free-stream pressure was needed for a corrected secondary flow ratio of 0.04. Later figures show that corrected secondary flow ratios of 0.02 and 0 are obtained with secondary total pressures equal to 96.5 and 95 percent of the ambient pressure. For the nonafterburning condition a corrected secondary flow ratio of 0.04 was obtained with a secondary total pressure equal to 96.7 percent of the ambient pressure.

For afterburning acceleration, figure 8(c) shows that the doors were closed at speeds above Mach number 0.85, and figure 8(b) shows that the flaps were fully open at speeds above Mach 1.5. This permitted the nozzle to operate near the fully expanded condition, and figure 8(a) shows that the nozzle efficiency was high throughout the acceleration speed range. The efficiency was lowest in the transonic range where the flaps were still partially closed and the boattail drag was high.

For the small primary configuration, figure 8(a) indicates that performance was very sensitive to nozzle pressure ratio as it was reduced from the acceleration value to typical subsonic cruise values. For example at Mach 0.85 or 0.90, reducing the pressure ratio from 5 or more, typical of acceleration, to about 4.2 caused about a 3-percent loss in efficiency. A further drop in pressure ratio to about 3.2 reduced the efficiency by an additional 2 to 3 percent to a value of about 87 percent. Figure 8(b) shows that the flaps tended to float further open at lower pressure ratios. As the pressure ratio was reduced from 4.20 to 3.27, the nozzle area ratio increased from 2.38 to 2.93. This increased the internal expansion and probably contributed to the reduction in efficiency. Figure 8(c) indicates that the tertiary doors were only slightly more than half open at a pressure ratio of 4.2. When the pressure ratio was reduced to 3.2 they opened further at a Mach number of 0.85, but remained at the same position at Mach 0.90. At these same conditions the secondary total pressure was a little less than ambient pressure

indicating that internal drag forces existed. This also would provide easy pumping of the secondary flow.

The small primary was also operated at Mach 2.0, the maximum wind tunnel speed, and near the design pressure ratio of 29.0 to obtain an approximate indication of supersonic cruise operation. With the difference in external flow effects between Mach 2.0 and 2.7 being relatively minor, the data are shown in the summary figure at Mach 2.7 the supersonic cruise Mach number. A nozzle efficiency of 0.971 was obtained at this condition with a pressure ratio of 27.6.

Floating Flap Position

The variation of boattail angle with nozzle pressure ratio over a range of Mach numbers is shown in figure 9. For the nonafterburning configuration (fig. 9(a)) the boattail angle was sensitive to free-stream Mach number and nozzle pressure ratio. At pressure ratios below 4.5, the flaps showed a stronger tendency to open as the free-stream Mach number increased from 0 to 0.9. This was probably responsible for the performance degradation at subsonic cruise conditions. With the doors and flaps closed the fully expanded nozzle pressure ratio is about 13.0. At subsonic Mach numbers, the boattail was closed at pressure ratios from 4.5 up to the maximum value tested of 7.0. However, at the supersonic Mach numbers, the flaps began opening between pressure ratios of 6 and 7 and were fully open at pressure ratios greater than 20.0. Supersonic flow over the boattail apparently reduced boattail pressures which resulted in an opening moment in spite of the internal overexpansion of the flow.

With the afterburning configuration (fig. 9(b)), the design pressure ratio with the flaps closed was about 7.0. The flaps began opening at pressure ratios near 6.0 for the supersonic Mach numbers and were fully open at nozzle pressure ratios greater than 10.5. At the subsonic Mach numbers the flaps opened at pressure ratios less than 2.5 and remained closed to the maximum pressure ratio tested (6.5). In addition to being sensitive to free-stream Mach number and nozzle pressure ratio, this configuration was also affected by the variations in corrected secondary flow rates up to 0.06 as indicated by the data band at a given Mach number and pressure ratio. In general, this occurred only at the transonic Mach numbers where the flaps were between the stops. Increases in secondary flow tended to close the flaps by pressurizing the cavity between the internal and external surfaces.

The flaps were stable at all simulated power settings and free-stream Mach numbers. The flaps had no friction built into their design other than that inherent in the linkage, and it was quite small.

Tertiary Door Position

The variation of tertiary door position with pressure ratio and Mach number is shown in figure 10. For the nonafterburning configuration (fig. 10(a)) the doors were generally closed at pressure ratios greater than 6.0. For the afterburning configuration (fig. 10(b)), they were closed at pressure ratios greater than 4.0. As will be seen in later figures, these pressure ratios correspond to the nozzle pumping characteristics providing secondary total pressures about equal to free-stream static pressure.

Small Primary Nozzle Performance

Nozzle efficiency and pumping characteristics at various Mach numbers from 0 to 1.97 and for a range of pressure ratios are shown in figure 11 for the nonafterburning configuration. Also presented on the figure is the boattail angle (when available) and whether the tertiary doors were full open (open symbols), in-travel (half-solid symbols) or closed (solid symbols). Tails on the performance points indicate that the secondary total pressure was less than free-stream static pressure ($P_s < p_0$) and, therefore, the secondary stream ideal thrust was set to zero. At conditions where the nozzle was charged with the ideal thrust of the secondary flow ($P_s > p_0$), peak efficiency generally occurred at a corrected secondary weight flow ratio of about 0.04; otherwise, the efficiency increased with secondary flow until P_s became larger than p_0, and the nozzle was then charged with the ideal secondary thrust.

At takeoff (fig. 11(a)) the nozzle operated with the doors full open and the flaps fully closed and obtained a relatively high efficiency at all pressure ratios. However, with subsonic external flow (figs. 11(b) to (f)) the performance was reduced below these high values. Typical nozzle operation with external flow can be seen in figure 11(e) at Mach 0.85. The tertiary doors never fully opened, even at a pressure ratio of 2.14. By comparing the solid symbols (doors closed) with the tailed symbols ($P_s < p_0$) it can be seen that the doors closed whenever the secondary total pressure became slightly larger than free-stream static pressure. Thus the doors closed at a pressure ratio of 6 to 7 which was about 1/2 the fully expanded pressure ratio with the boattail closed. At pressure ratios appropriate for subsonic cruise (3.20 and 4.25), secondary total pressure was less than the free-stream static value as indicated by the tailed symbols, and this caused low pressures in the region of the primary nozzle base.

These low internal pressures can be seen in table I which presents listings of the static pressures at various conditions from Mach 0 to 0.9. At Mach numbers 0.85 and 0.9, and with subsonic cruise pressure ratios, the internal nozzle static pressures in the primary base region averaged about 5 percent less than free-stream static pressure,

indicating relatively high drag forces. Pressures on the 3° fixed boattail indicated that little drag existed in this region, but static pressures on the floating boattail indicated drag on the outer portion of it. However, the 3° boattail pressures may be somewhat misleading since the orifice was located directly downstream of a tertiary door and may not be representative of the average boattail pressure. At a higher pressure ratio (7.29) when the doors are closed (table I(c)) the 3° boattail statics indicated a lower pressure and thus a higher drag. These lower pressures could also exist in between doors when the doors are open. At this same nozzle pressure ratio, table I(c) also shows internal pressures in the primary nozzle base region which were above free-stream static pressure indicating internal thrust at this condition.

A limited amount of data were taken for the nonafterburning configuration at Mach numbers 1.20 and 1.47. These efficiencies are shown in figure 12 as a function of nozzle pressure ratio for a corrected secondary weight flow ratio of 0.06. A summary of the effect of nozzle pressure ratio on nozzle efficiency for a constant corrected secondary weight flow ratio of 0.04 is shown in figure 13 for various Mach numbers. The nozzle gross thrust coefficients for various Mach numbers and nozzle pressure ratios are shown in figure 14.

Large Primary Nozzle Performance

The nozzle efficiency and pumping characteristics at various Mach numbers and pressure ratios are given in figure 15 for the afterburning primary nozzle. The nozzle efficiency generally peaked between 0.04 and 0.06 corrected secondary weight flow ratio. The nozzle efficiency was generally 3 percent better than the nonafterburning configuration due to a reduction in overexpansion losses. In addition the primary thrust was larger thereby reducing the relative effect of boattail drag on performance.

Because of the small number of data points taken at the idle descent power setting and because of the random variations in secondary flow at this power setting, the idle descent performance is listed separately in table II.

The effect of nozzle pressure ratio on nozzle efficiency for a constant corrected secondary weight flow ratio of 0.04 is shown in figure 16 for various Mach numbers. The nozzle gross thrust coefficients for various Mach numbers and nozzle pressure ratios are shown in figure 17.

Nozzle Pumping Characteristics

The pressure recovery requirements for the secondary system are shown in figure 18. At subsonic cruise power settings (fig. 18(a)), the secondary total pressure

required for a corrected secondary weight flow ratio of 0.04 was only 0.55 of the free-stream total pressure at Mach 0.9. At subsonic speeds with higher power settings the pressure recovery became a little more critical. For example, with the nonafterburning acceleration power setting at Mach 0.41 (fig. 18(b)), a secondary total pressure of 0.88 of free-stream total pressure was required for a corrected secondary weight flow ratio of 0.04. These pumping curves were relatively flat and reduced secondary flow rates would not affect the pressure recovery requirements appreciably. For the afterburning acceleration power setting at Mach 0.9 (fig. 18(c)), a secondary total pressure of 0.70 of free-stream total pressure was required for a corrected secondary weight flow ratio of 0.04. At takeoff, secondary flow pumping was marginal. A secondary pressure equal to free-stream pressure was needed to pump a secondary flow ratio of 0.04. Corrected secondary weight flow ratios of 0.02 and 0 were obtained with secondary total pressures equal to 96.5 and 95 percent of the ambient pressure. Results obtained at Mach 1.97 are shown in figure 18(d).

Nozzle Modification

As discussed earlier the nonafterburning configuration was modified and tested at increased corrected secondary flow rates of up to 0.16 in an attempt to force the flaps closed at subsonic cruise conditions, thereby reducing the overexpansion losses. The resulting boattail angles as a function of nozzle pressure ratio are presented in figure 19. Comparing the solid and open symbols in figure 19, it can be seen that the configuration changes did not significantly affect the boattail angle. At the subsonic cruise Mach numbers the flaps were still partially open at pressure ratios below approximately 4.5.

The nozzle efficiency and pumping characteristics for the three modified configurations are shown in figures 20 to 22 for the Mach numbers investigated. In general, configurations 1 and 2 performed in a similar manner. At Mach 0.4 nozzle efficiency was improved from 1 to 2 percent. At the subsonic cruise Mach numbers the efficiency was the same or less than the unmodified nonafterburning configuration. Configuration 3 had much lower nozzle efficiency at all three Mach numbers. This configuration, with the annular air guide slot plugged, was tested primarily to determine whether directing all of the secondary flow into the secondary flap cavity would pressurize the cavity enough to close the flaps at subsonic cruise. However, there was no appreciable change in the flap position.

SUMMARY OF RESULTS

An experimental investigation was conducted to determine the performance characteristics of an auxiliary inlet ejector with aerodynamically positioned tertiary doors and secondary flaps at Mach numbers from 0 to 2.0. Two primary nozzles were tested: a small nozzle with a throat to nacelle area ratio of 0.185 to simulate a configuration for subsonic and supersonic cruise and nonafterburning acceleration, and a large nozzle with a throat to nacelle area ratio of 0.261 to simulate a configuration for afterburning takeoff and acceleration and for idle descent. The following general trends were indicated:

1. At takeoff nozzle efficiencies of 0.980 and 0.982 were obtained with the large and small primary nozzles at pressure ratios near 3.0. The flaps were fully closed and the doors fully open. Secondary flow pumping was marginal for the large primary since a secondary pressure equal to free-stream pressure was needed to pump a corrected secondary weight flow ratio of 0.04.

2. At subsonic cruise both nozzle performance and floating flap position were sensitive to nozzle pressure ratio. At Mach 0.9 increasing pressure ratio from 3.27 to 4.20 increased nozzle efficiency about 2 percent to 0.888 and decreased the nozzle area ratio from 2.93 to 2.38.

3. At Mach 2.0 and with a nozzle pressure ratio of 27.6, the small primary nozzle had an efficiency of 0.971 with the flaps fully open and the doors fully closed.

4. The aerodynamically positioned flaps (which could reduce the exit area by 38 percent) were stable at all simulated power settings and free-stream Mach numbers. The flaps were fully open at pressure ratios greater than 20 for the small primary and at pressure ratios greater than 10.5 for the large primary. At lower pressure ratios the floating position was sensitive to free-stream Mach number and to secondary flow. Free-stream effects were most prominent at subsonic speeds at pressure ratios less than 4.0.

5. For a typical trajectory the flaps would be closed at takeoff and during subsonic acceleration. The flaps begin to open at Mach 1.0 and are fully opened at Mach numbers of 1.47 and above.

6. The auxiliary inlets were open at takeoff and partially open at subsonic cruise. During acceleration the inlets were closed at speeds above Mach 0.8.

Lewis Research Center,
National Aeronautics and Space Administration,
Cleveland, Ohio, February 25, 1970,
720-03.

REFERENCES

1. Bresnahan, Donald L.: Experimental Investigation of a 10° Conical Turbojet Plug Nozzle With Iris Primary and Translating Shroud at Mach Numbers from 0 to 2.0. NASA TM X-1709, 1968.
2. Steffen, Fred W.; and Jones, John R.: Performance of a Wind Tunnel Model of an Aerodynamically Positioned Variable Flap Ejector at Mach Numbers from 0 to 2.0. NASA TM X-1639, 1968.
3. Shrewsbury, George D.; and Jones, John R.: Static Performance of an Auxiliary Inlet Ejector Nozzle for Supersonic-Cruise Aircraft. NASA TM X-1653, 1968.
4. Lauer, Rodney F., Jr.; and Mercer, Charles E.: Blow-In-Door Ejector Nozzle Performance Comparison Between Fixed-Open and Free-Floating Door Configurations. NASA TM X-1177, 1967.
5. Smith, K. G.: Methods and Charts for Estimating Skin Friction Drag in Wind Tunnel Tests With Zero Heat Transfer. Rep. ARC CP-824, Aeronautical Research Council, Great Britain, 1965. (Available from DDC as AD-487132.)
6. Harrington, Douglas E.: Jet Effects on Boattail Pressure Drag of Isolated Ejector Nozzles at Mach Numbers from 0.60 to 1.47. NASA TM X-1785, 1969.
7. Mitchell, Glenn A.: Effect of Model Forebody Shape on Perforated Tunnel Wall Interference. NASA TM X-1656, 1968.

TABLE I. - RATIOS OF LOCAL PRESSURES TO FREE-STREAM STATIC PRESSURE

FOR NONAFTERBURNING CONFIGURATION

(a) Free-stream Mach number, 0; boattail angle, $\beta = 16.2^{\circ}$; nozzle exit to nozzle throat area ratio, $A_9/A_8 = 2.23$

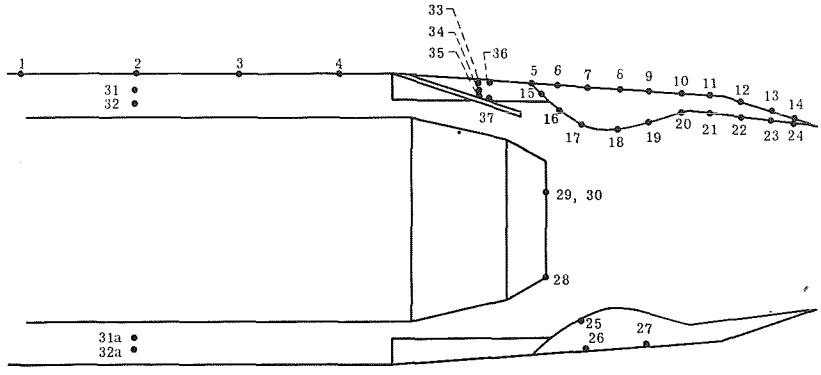

(a-1) Nozzle pressure ratio, $P_7/p_0 = 3.09$; corrected secondary weight flow ratio, $\omega\sqrt{\tau} = 0.0406$; nozzle efficiency, $(F - D)/(F_{ip} + F_{is}) = 0.982$

Orifice	Local to free-stream static pressure, p_x/p_0	Orifice	Local to free-stream static pressure, p_x/p_0
1	0.999	25	-----
2	.999	26	0.952
3	.996	27	.953
4	.997		
5	.999	28	.949
6	.997	29	.951
7	.999	30	-----
8	1.000		
9	-----	31	.970
10	.968	32	.970
11	.999		
12	.999	31a	.970
13	1.006	32a	.973
14	.999		
		33	.966
15	.948	34	.967
16	.948	35	.966
17	.930		
18	.906	36	.965
19	.929	37	.967
20	.932		
21	.936		
22	.936		
23	.958		
24	.970		

(a-2) Nozzle pressure ratio, $P_7/p_0 = 3.60$; corrected secondary weight flow ratio, $\omega\sqrt{\tau} = 0.041$; nozzle efficiency, $(F - D)/(F_{ip} + F_{is}) = 0.980$

Orifice	Local to free-stream static pressure, p_x/p_0	Orifice	Local to free-stream static pressure, p_x/p_0
1	0.999	25	-----
2	.999	26	0.941
3	.996	27	.942
4	.996		
5	1.000	28	.941
6	.997	29	.943
7	.999	30	-----
8	1.000		
9	-----	31	.968
10	-----	32	.968
11	.999		
12	.999	31a	.969
13	1.005	32a	.973
14	.998		
		33	.963
15	.941	34	.965
16	.938	35	.964
17	.906		
18	.858	36	.962
19	.891	37	.965
20	.908		
21	.925		
22	.933		
23	.958		
24	.966		

TABLE I. - Continued. RATIOS OF LOCAL PRESSURES TO FREE-STREAM STATIC PRESSURE FOR NONAFTERBURNING CONFIGURATION

(b) Free-stream Mach number, 0.85

(b-1) Nozzle pressure ratio, P_7/p_0 = 3.20; corrected secondary weight flow ratio, $\omega\sqrt{\tau}$ = 0.0388; nozzle efficiency, $(F - D)/(F_{ip} + F_{is})$ = 0.878; boattail angle, $\beta = 10^{\circ}$; nozzle exit to nozzle throat area ratio, A_9/A_8 = 2.78

Orifice	Local to free-stream static pressure, p_x/p_0	Orifice	Local to free-stream static pressure, p_x/p_0
1	0.983	25	0.953
2	.975	26	.946
3	.959	27	.950
4	.935		
5	1.030	28	.945
6	1.013	29	.945
7	1.002	30	-----
8	.998		
9	-----	31	.954
10	.943	32	.950
11	.951		
12	.950	31a	.952
13	-----	32a	.958
14	1.027		
		33	.950
15	1.040	34	.950
16	.942	35	.950
17	.872		
18	.805	36	.946
19	.885	37	.950
20	.935		
21	.942		
22	.956		
23	.982		
24	.948		

(b-2) Nozzle pressure ratio, P_7/p_0 = 4.25; corrected secondary weight flow ratio, $\omega\sqrt{\tau}$ = 0.0466; nozzle efficiency, $(F - D)/(F_{ip} + F_{is})$ = 0.906; boattail angle, $\beta = 15^{\circ}$; nozzle exit to nozzle throat area ratio, A_9/A_8 = 2.35

Orifice	Local to free-stream static pressure, p_x/p_0	Orifice	Local to free-stream static pressure, p_x/p_0
1	0.984	25	0.954
2	.976	26	.954
3	.962	27	.956
4	.940		
5	1.015	28	.953
6	.999	29	.949
7	.988	30	-----
8	.984		
9	-----	31	.974
10	.965	32	.976
11	.926		
12	.908	31a	.978
13	-----	32a	.984
14	1.064		
		33	.970
15	1.039	34	.972
16	.952	35	.972
17	.874		
18	.768	36	.966
19	.800	37	.970
20	.898		
21	.938		
22	.958		
23	1.004		
24	.971		

TABLE I. - Concluded. RATIOS OF LOCAL PRESSURES TO FREE-STREAM STATIC PRESSURE

FOR NONAFTERBURNING CONFIGURATION

(c) Free-stream Mach number, 0.90

(c-1) Nozzle pressure ratio, P_7/p_0 = 3.27; corrected secondary weight flow ratio, $\omega\sqrt{\tau}$ = 0.042; nozzle efficiency, $(F - D)/(F_{ip} + F_{is})$ = 0.868; boattail angle, β = 8.5°; nozzle exit to nozzle throat area ratio, A_9/A_8 = 2.93

Orifice	Local to free-stream static pressure, p_x/p_0	Orifice	Local to free-stream static pressure, p_x/p_0
1	0.983	25	-----
2	.974	26	0.938
3	.957	27	.943
4	.929		
5	1.032	28	.923
6	1.013	29	.923
7	1.000	30	-----
8	.994		
9	-----	31	.943
10	.927	32	.940
11	.935		
12	.926	31a	.943
13	-----	32a	.950
14	1.020		
		33	.939
15	1.025	34	.940
16	.923	35	.939
17	.868		
18	.841	36	.936
19	.901	37	.938
20	.933		
21	.943		
22	.953		
23	.973		
24	.933		

(c-2) Nozzle pressure ratio, P_7/p_0 = 4.20; corrected secondary weight flow ratio, $\omega\sqrt{\tau}$ = 0.048; nozzle efficiency, $(F - D)/(F_{ip} + F_{is})$ = 0.894; boattail angle, β = 14.5°; nozzle exit to nozzle throat area ratio, A_9/A_8 = 2.38

Orifice	Local to free-stream static pressure, p_x/p_0	Orifice	Local to free-stream static pressure, p_x/p_0
1	0.983	25	-----
2	.975	26	0.945
3	.958	27	.949
4	.931		
5	1.017	28	.935
6	1.000	29	.931
7	.988	30	-----
8	.983		
9	-----	31	.960
10	.950	32	.960
11	.914		
12	.888	31a	.964
13	-----	32a	.972
14	1.055		
		33	.956
15	1.027	34	.958
16	.935	35	.958
17	.858		
18	.774	36	.953
19	.825	37	.957
20	.917		
21	.938		
22	.960		
23	.993		
24	.955		

(c-3) Nozzle pressure ratio, P_7/p_0 = 7.29; corrected secondary weight flow ratio, $\omega\sqrt{\tau}$ = 0.059; nozzle efficiency, $(F - D)/(F_{ip} + F_{is})$ = 0.936; boattail angle, β = 16.25°; nozzle exit to nozzle throat area ratio, A_9/A_8 = 2.24

Orifice	Local to free-stream static pressure, p_x/p_0	Orifice	Local to free-stream static pressure, p_x/p_0
1	0.986	25	-----
2	.979	26	1.030
3	.966	27	1.030
4	.949		
5	.954	28	1.045
6	.957	29	1.049
7	.956	30	-----
8	.958		
9	.946	31	1.115
10	-----	32	1.203
11	.918		
12	.884	31a	1.145
13	-----	32a	1.152
14	1.026		
		33	1.108
15	1.042	34	1.114
16	1.042	35	1.112
17	1.028		
18	.992	36	1.106
19	.977	37	1.111
20	-----		
21	.955		
22	.890		
23	.788		
24	1.115		

TABLE II. - IDLE DESCENT PERFORMANCE

LARGE PRIMARY

Free-stream Mach number, M_0	Nozzle pressure ratio, P_7/p_0	Nozzle efficiency, $\frac{F - D}{F_{ip} + F_{is}}$	Corrected secondary weight flow ratio, $\omega\sqrt{\tau}$	Secondary to primary total pressure ratio, P_s/P_7	Ratio of secondary total pressure to free-stream total pressure, P_s/P_0.
0.41	1.08	0.734	0.10	0.92	0.888
.41	1.29	.906	.13	.78	.901
.85	1.17	.718	.13	.86	.625
.85	1.40	.853	.13	.73	.630
.90	1.33	.825	.14	.76	.598
.90	1.61	.860	.14	.64	.608
1.00	1.43	.729	.14	.72	.540
1.00	1.72	.806	.14	.61	.546
1.20	1.57	.674	.15	.60	.399
1.20	2.10	.700	.14	.46	.397
1.47	2.27	.803	.16	.47	.304
1.77	3.04	.719	.15	.40	.223
1.97	4.99	.854	.15	.37	.250

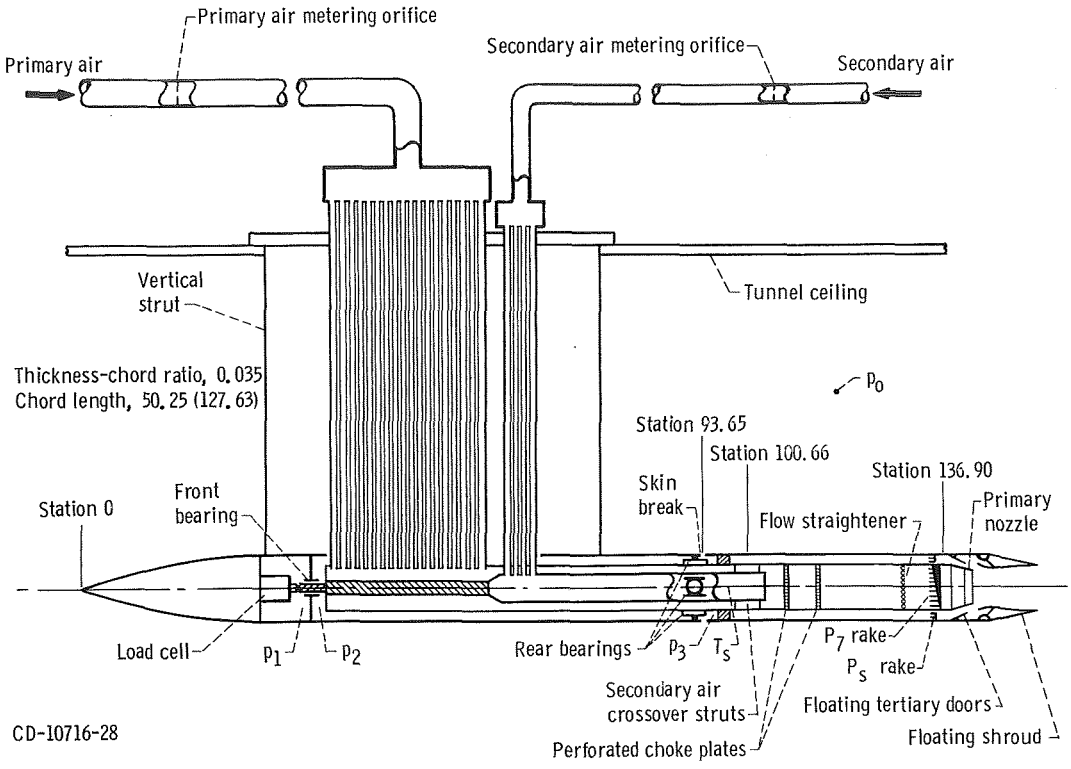

Figure 1. - Nozzle support model and air supply systems for 8-by-6 supersonic wind tunnel tests. (Dimensions are in inches (cm).)

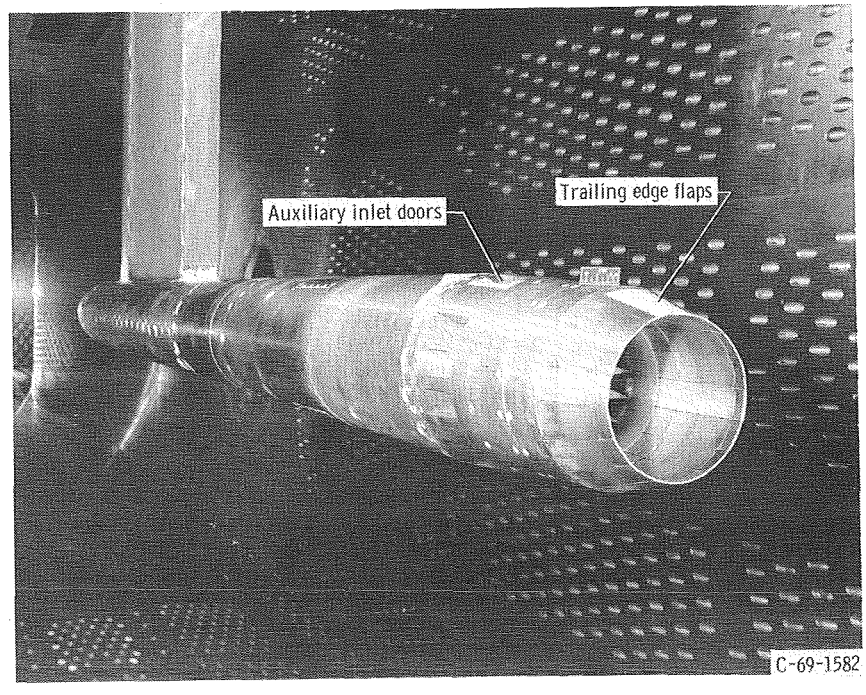

Figure 2. - Installation of nozzle in 8- by 6-Foot Supersonic Wind Tunnel.

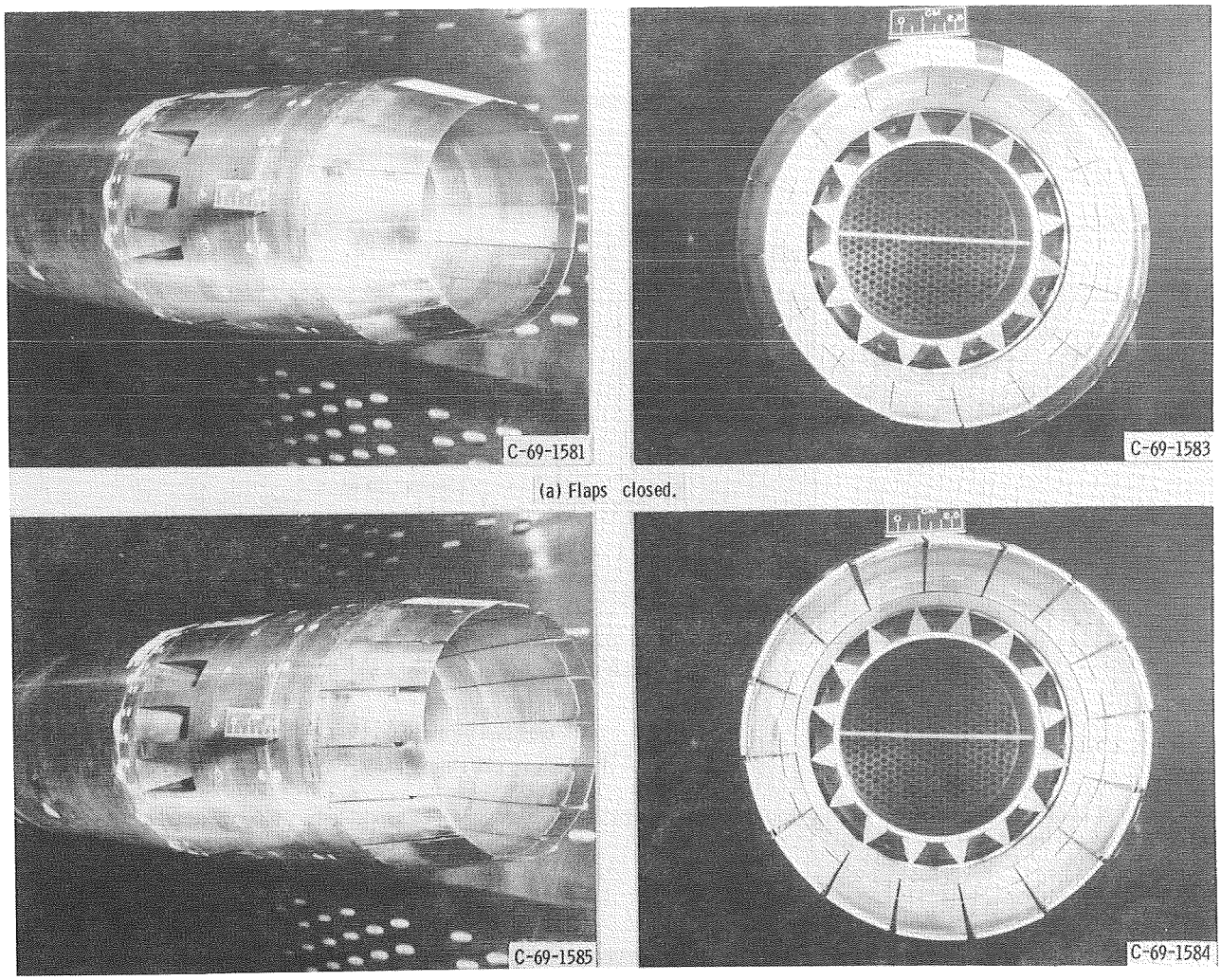

(a) Flaps closed.

(b) Flaps open.

Figure 3. - Auxiliary inlet ejector nozzle.

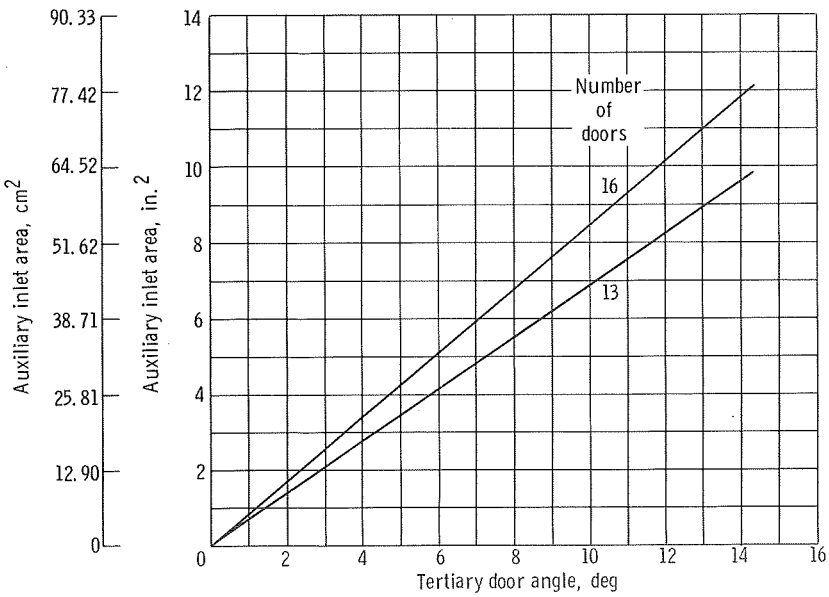

Figure 4. - Auxiliary inlet area as function of tertiary door angle.

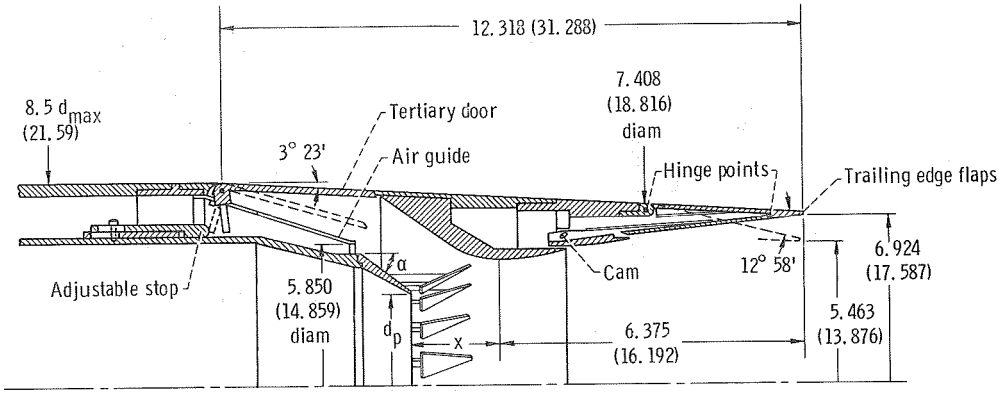

	Primary diameter, d_p,		External primary nozzle angle, α, deg	Axial distance, x		Nozzle flow coefficient, C_d
	in.	cm		in.	cm	
Nonafterburning configuration	3.660	9.264	37	1.9365	4.919	0.944
Afterburning configuration	4.341	11.026	22	1.8125	4.604	.972

(a) Basic model dimensions.

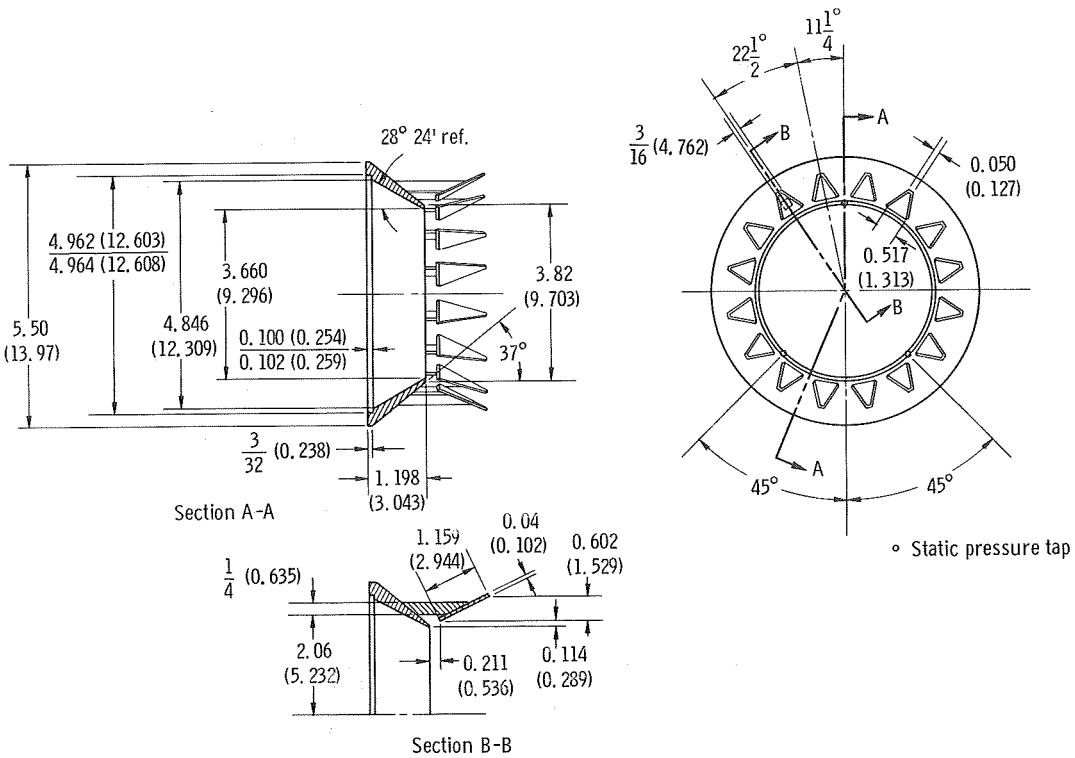

(b) Small primary.

Figure 5. - Model dimensions and geometric variables. (Dimensions are in inches (cm) unless otherwise noted).

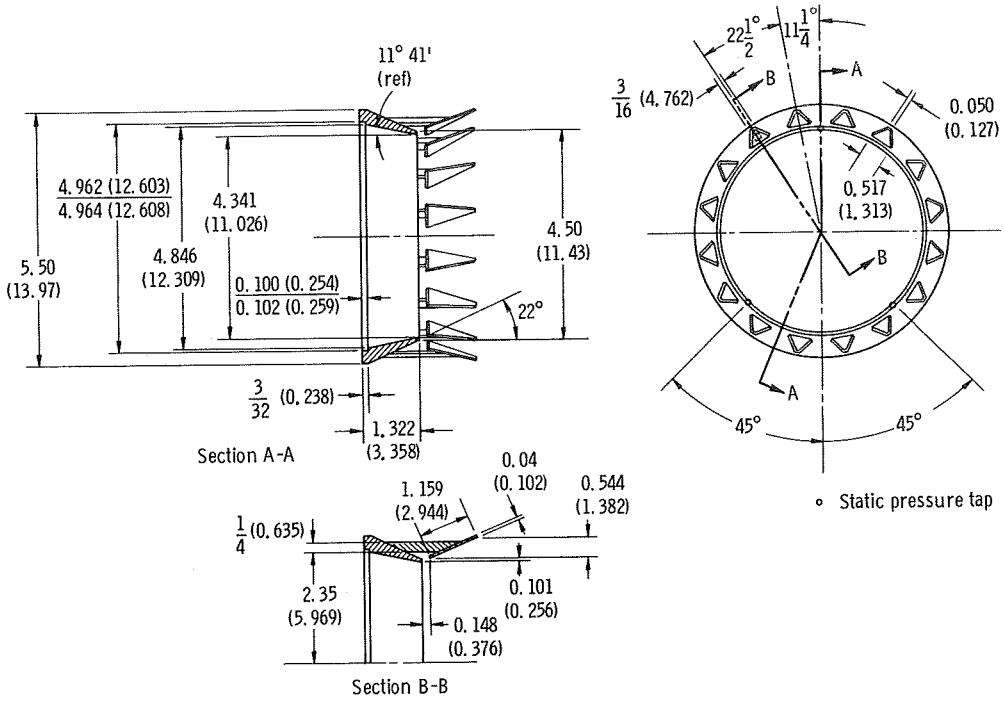

(c) Large primary.

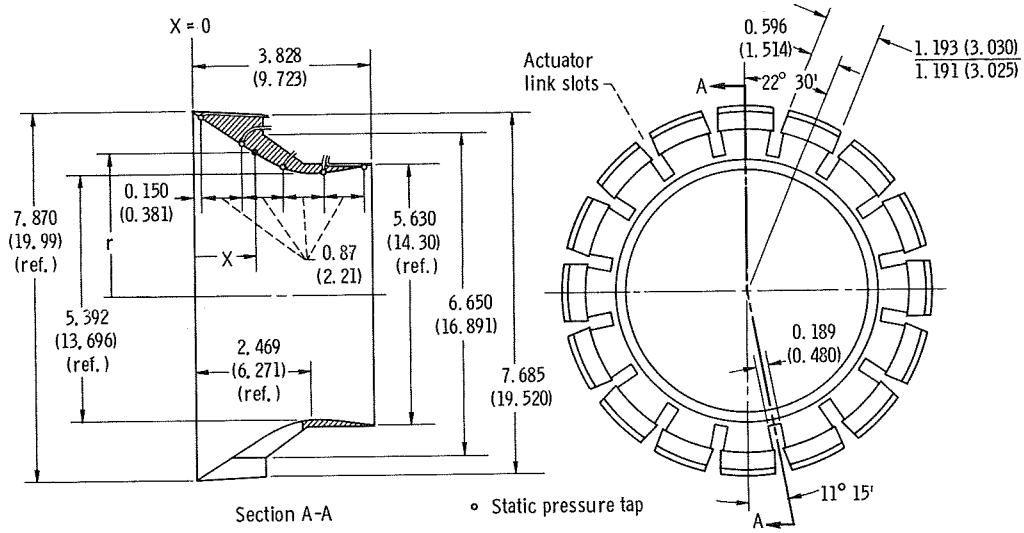

Axial distance, x		Radius, r		Axial distance, x		Radius, r	
in.	cm	in.	cm	in.	cm	in.	cm
0	0	3.935	9.995	2.250	5.715	2.704	6.868
.250	.635	3.780	9.601	2.469	6.271	2.696	6.848
.500	1.270	3.614	9.179	2.500	6.350	2.696	6.848
.750	1.905	3.434	8.722	2.750	6.985	2.700	6.858
1.000	2.54	3.245	8.242	3.000	7.62	2.715	6.896
1.250	3.175	3.058	7.767	3.250	8.255	2.735	6.947
1.500	3.810	2.918	7.412	3.500	8.890	2.766	7.026
1.750	4.445	2.815	7.150	3.750	9.525	2.804	7.122
2.000	5.08	2.744	6.970	3.828	9.723	2.815	7.150

(d) Forward secondary.

Figure 5. - Continued.

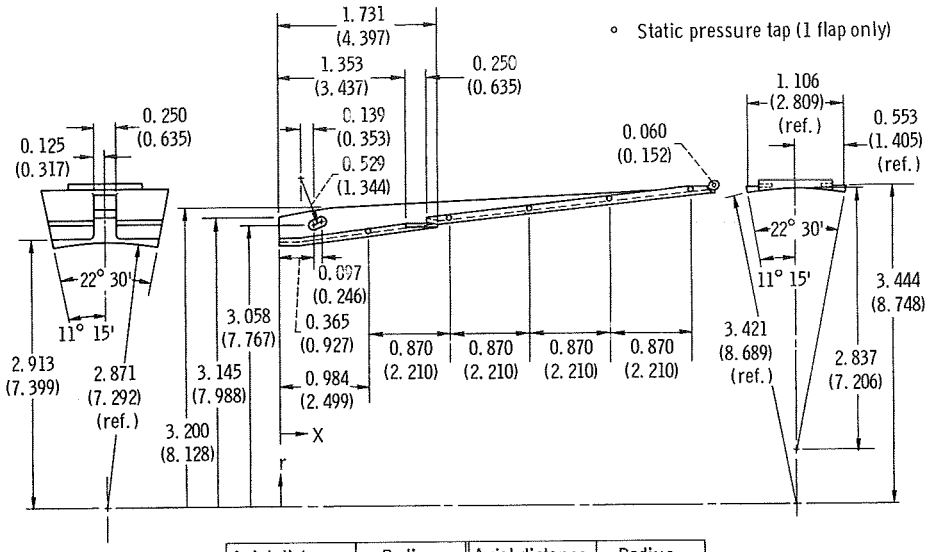

Axial distance, x		Radius, r		Axial distance, x		Radius, r	
in.	cm	in.	cm	in.	cm	in.	cm
0.312	0.792	2.871	7.292	2.488	6.319	3.201	8.130
.596	1.514	2.915	7.404	2.866	7.280	3.246	8.245
.974	2.474	2.970	7.544	3.244	8.240	3.289	8.354
1.353	3.437	3.020	7.671	3.623	9.202	3.328	8.453
1.731	4.397	3.067	7.790	4.001	10.162	3.362	8.539
1.731	4.397	3.098	7.869	4.379	11.122	3.393	8.618
2.109	5.357	3.152	8.006	4.758	12.077	3.421	8.689

(e) Inner flap.

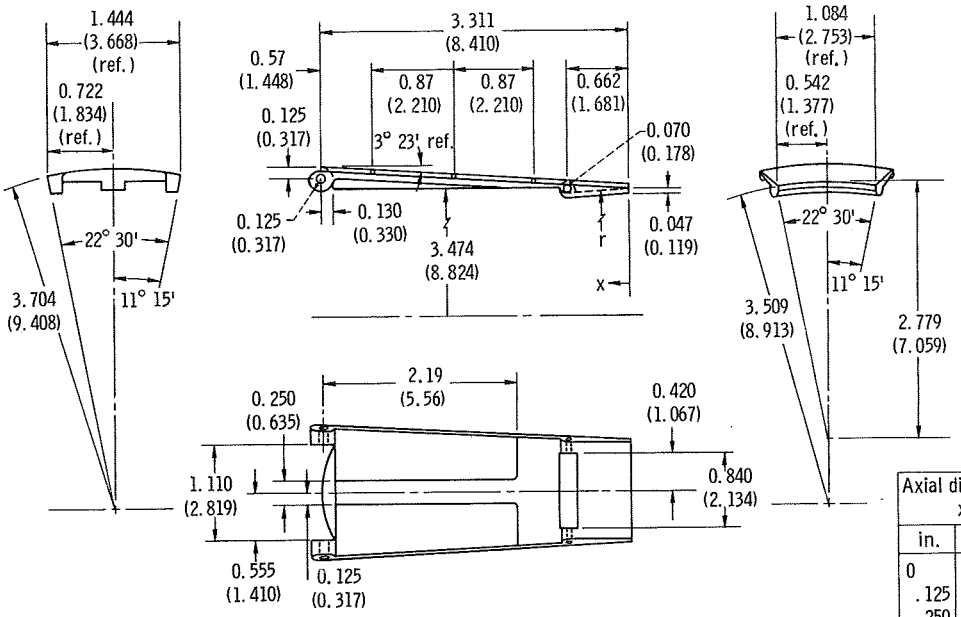

Axial distance, x		Radius, r	
in.	cm	in.	cm
0	0	3.462	8.793
.125	.317	3.455	8.776
.250	.635	3.448	8.758
.375	.952	3.441	8.740
.500	1.270	3.433	8.720
.662	1.681	3.421	8.689

(f) Outer flap.

Figure 5. - Continued.

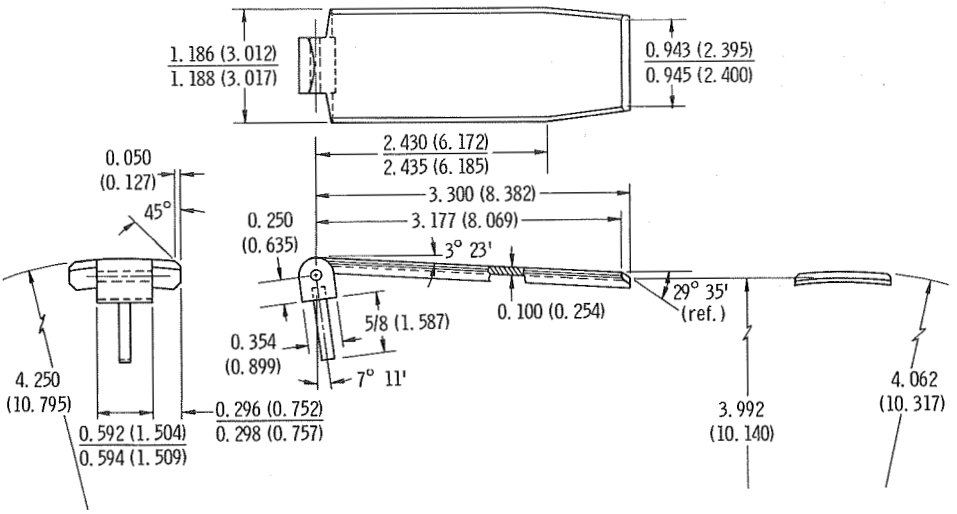

(g) Tertiary door.

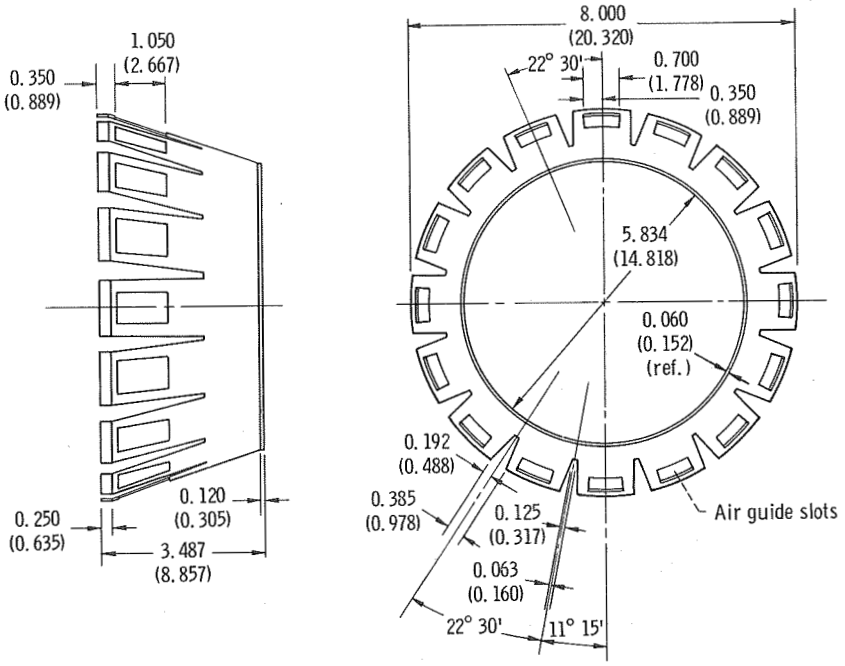

(h) Air guide.

Figure 5. - Continued.

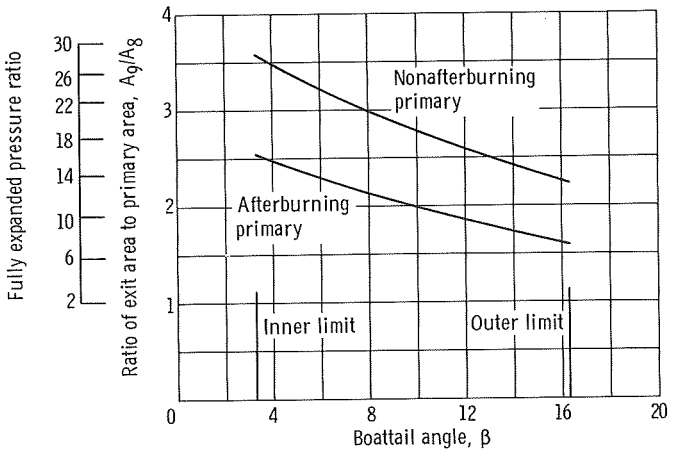

(i) Variation of geometric nozzle area ratio with boattail angle.

Figure 5. - Concluded.

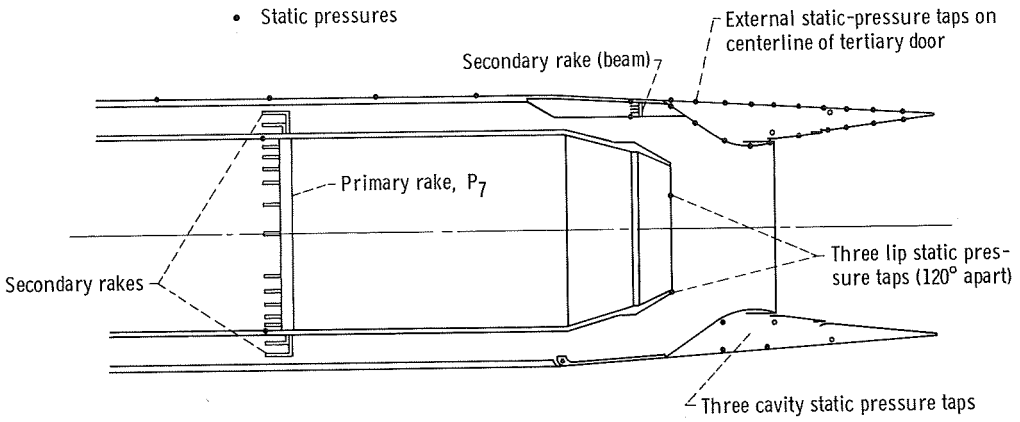

(a) Total and static pressure measurement locations.

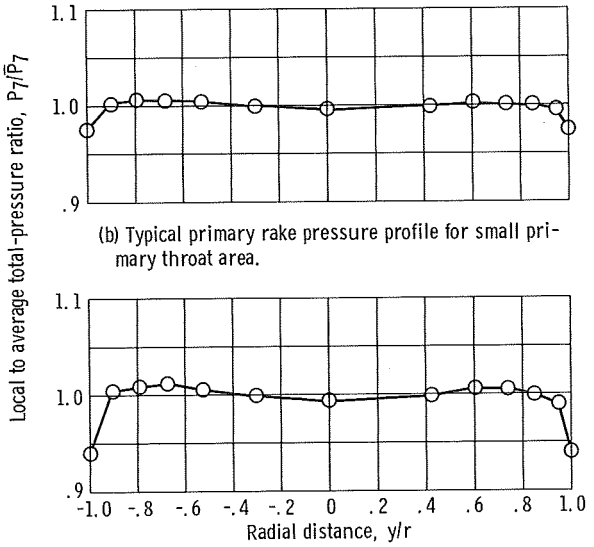

(b) Typical primary rake pressure profile for small primary throat area.

(c) Typical primary rake pressure profile for large primary throat area.

Figure 6. - Model instrumentation.

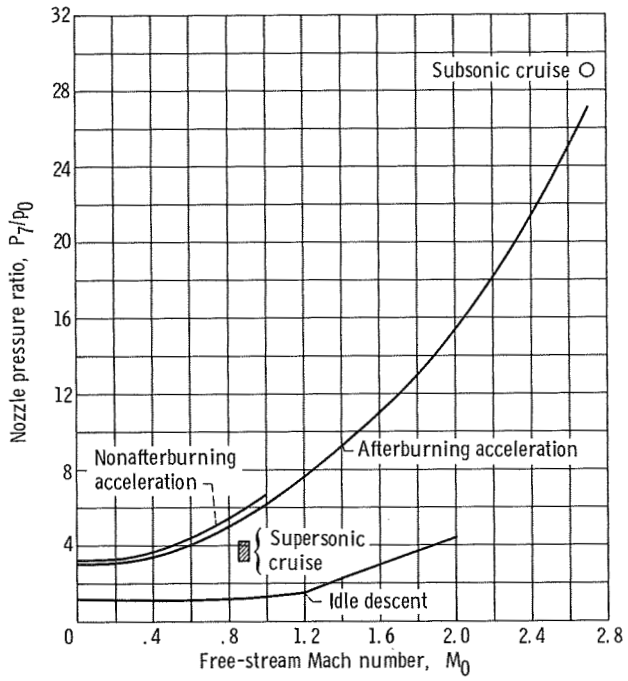

Figure 7. - Schedule of nozzle pressure ratio with free-stream Mach number for simulated power settings.

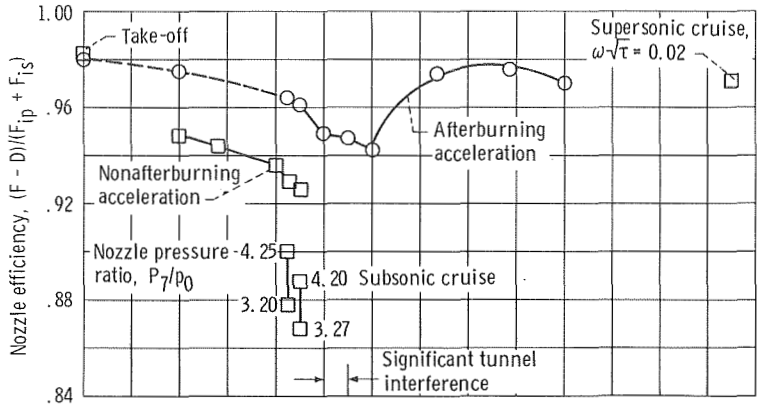

(a) Nozzle efficiency.

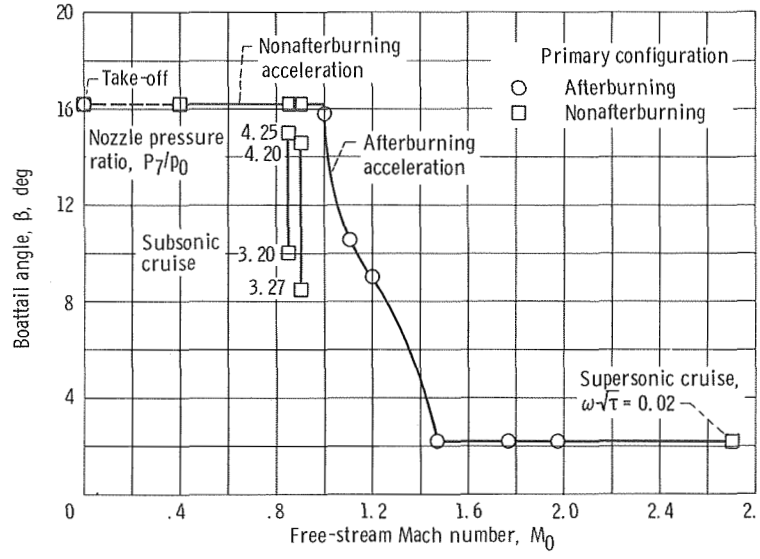

(b) Variation of boattail angle with Mach number.

Figure 8. - Performance of auxiliary inlet ejector over flight Mach number range at nominal $\omega\sqrt{\tau} = 0.04$.

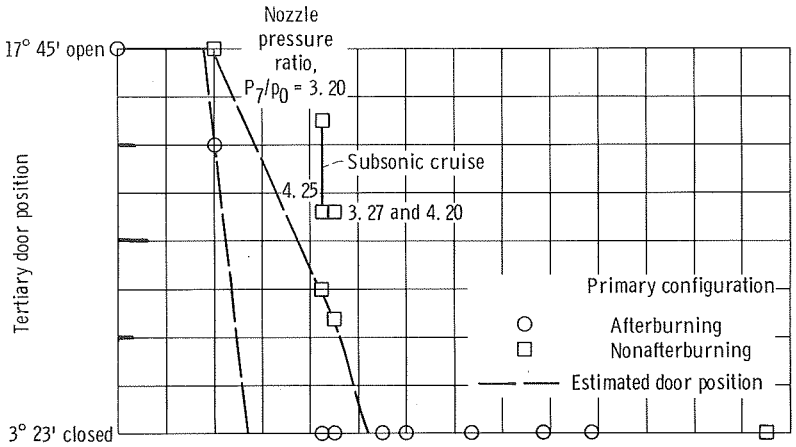

(c) Variation of tertiary door position with Mach number.

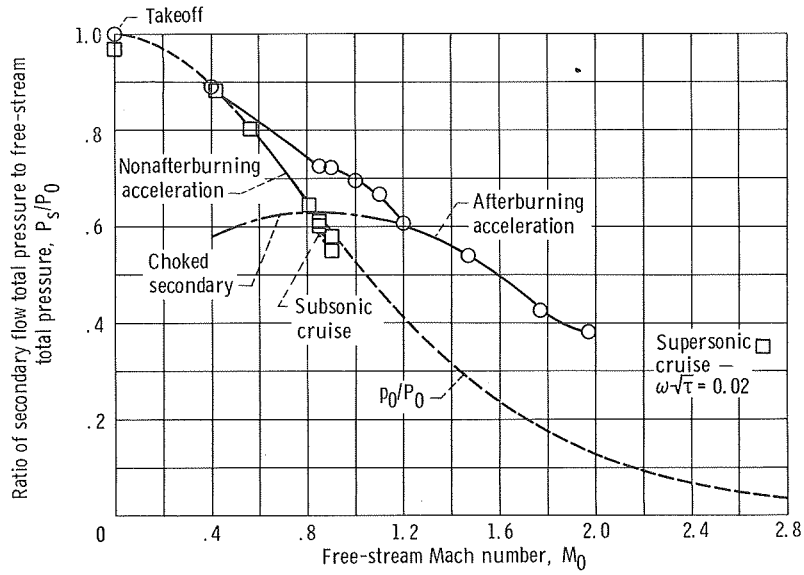

(d) Secondary total pressure recovery requirements.

Figure 8. - Concluded.

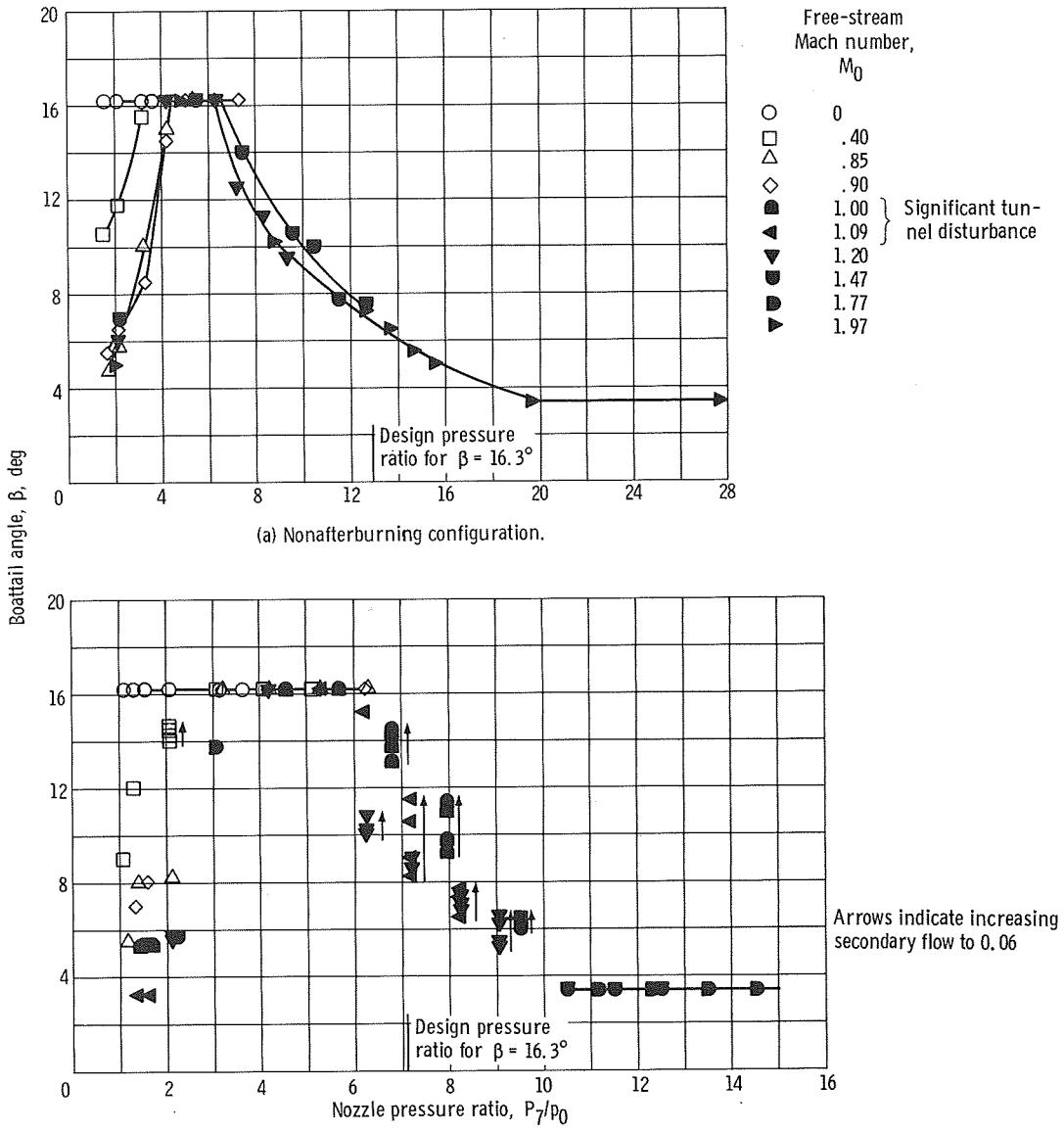

(a) Nonafterburning configuration.

(b) Afterburning configuration.

Figure 9. - Variation of boattail angle with nozzle pressure ratio over range of free-stream Mach numbers.

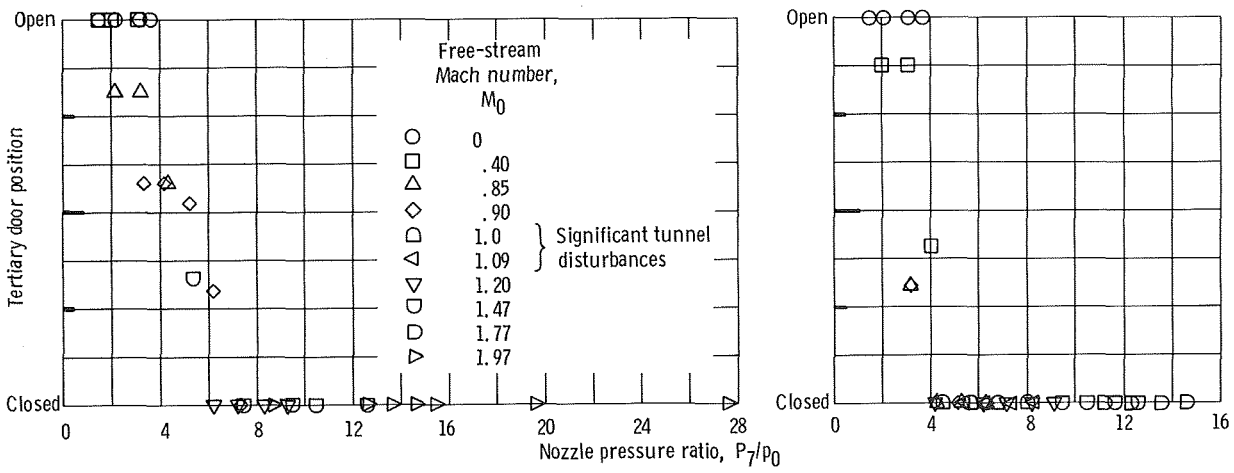

(a) Nonafterburning configuration.

(b) Afterburning configuration.

Figure 10. - Variation of tertiary door position with nozzle pressure ratio over range of free-stream Mach numbers, $\omega\sqrt{\tau} = 0.04$.

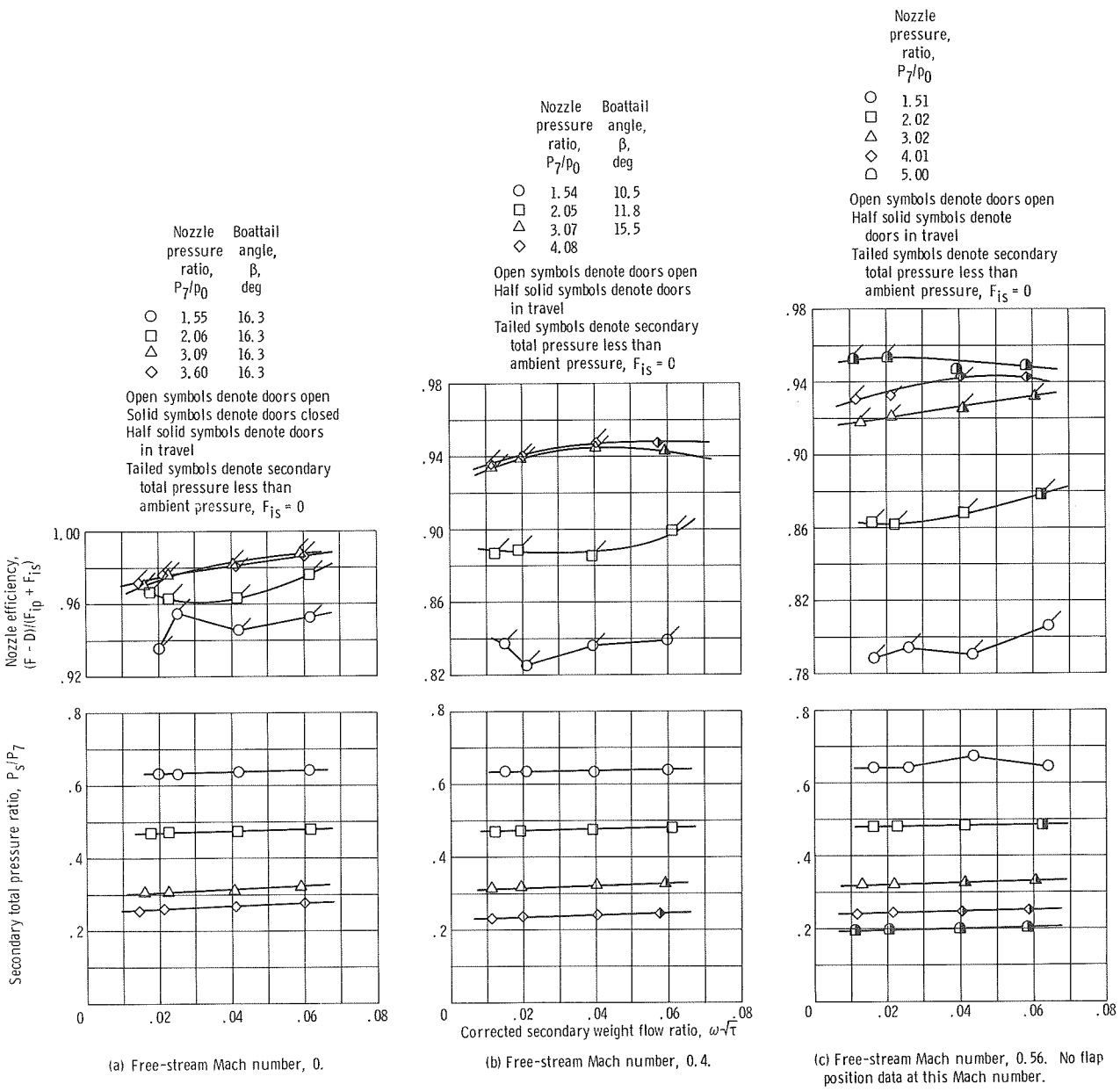

(a) Free-stream Mach number, 0.

(b) Free-stream Mach number, 0.4.

(c) Free-stream Mach number, 0.56. No flap position data at this Mach number.

Figure 11. - Nozzle efficiency and pumping characteristics as function of corrected secondary weight flow ratio for small primary.

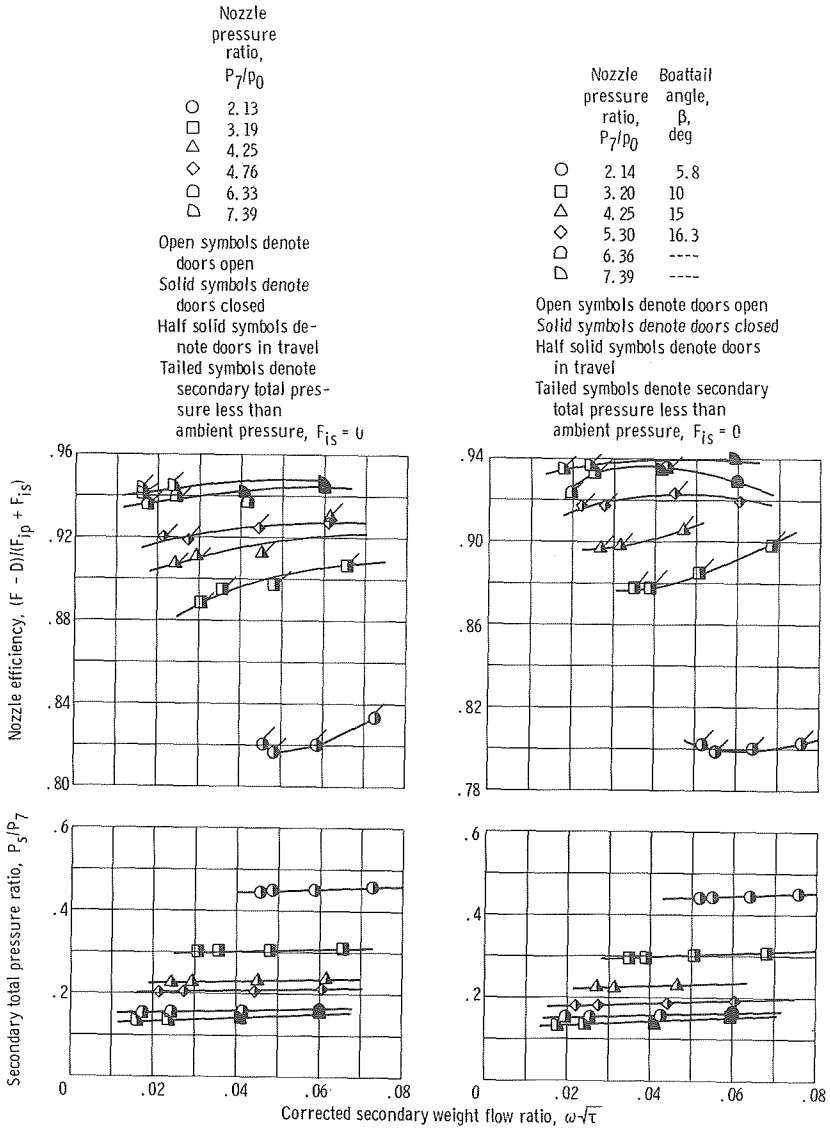

(d) Free-stream Mach number, 0.8. No flap position data at this Mach number.

(e) Free-stream Mach number, 0.85.

Figure 11. - Continued.

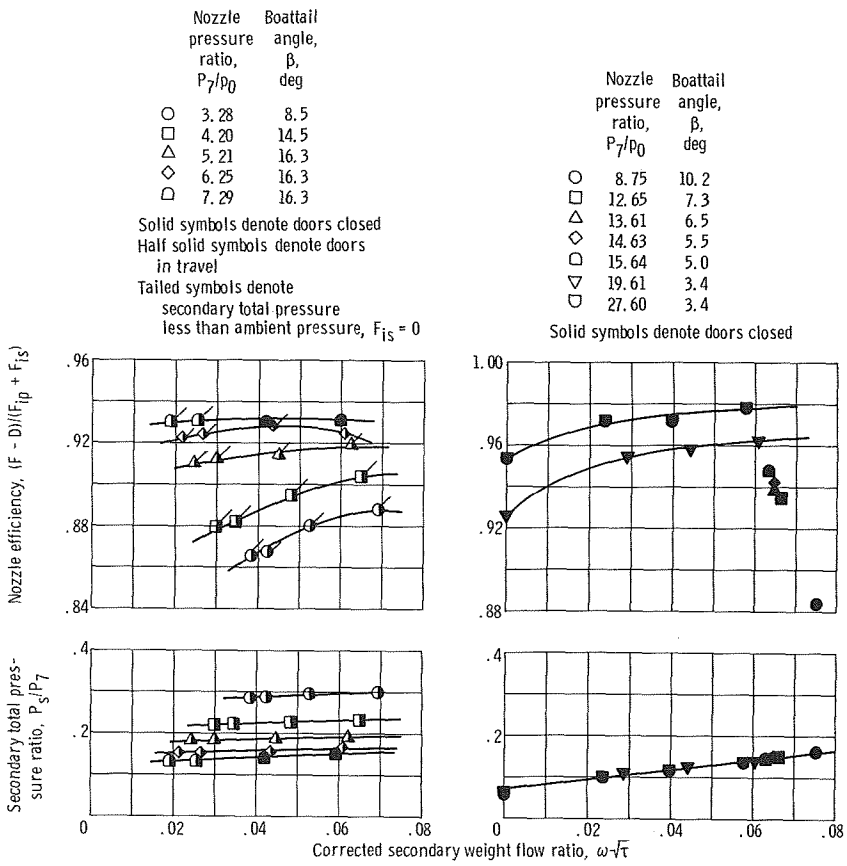

(f) Free-stream Mach number, 0.9.

(g) Free-stream Mach number, 1.97.

Figure 11. - Concluded.

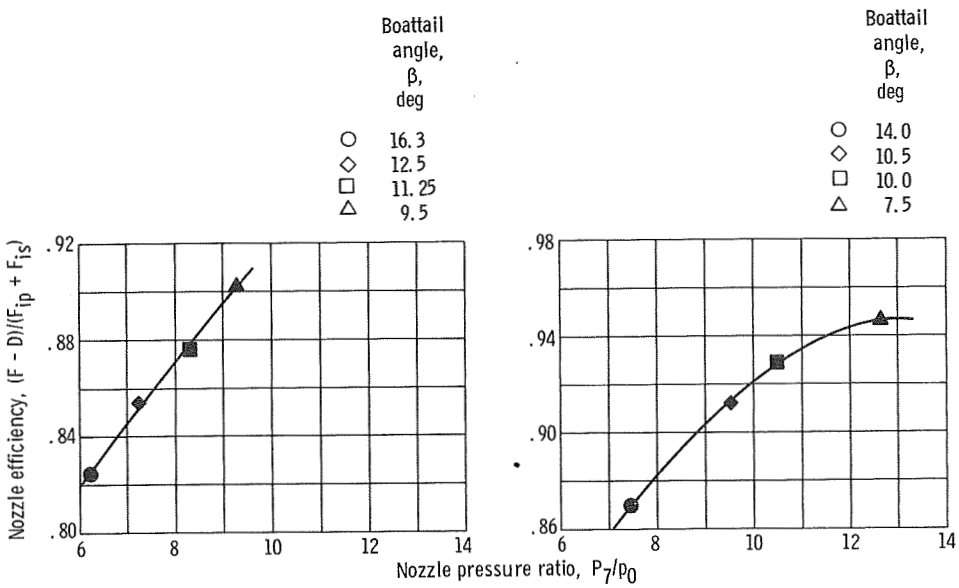

(a) Free-stream Mach number, 1.20.

(b) Free-stream Mach number, 1.47.

Figure 12. - Nozzle efficiency as function of nozzle pressure ratio for small primary with corrected secondary weight flow ratio of 0.06. Doors fully closed.

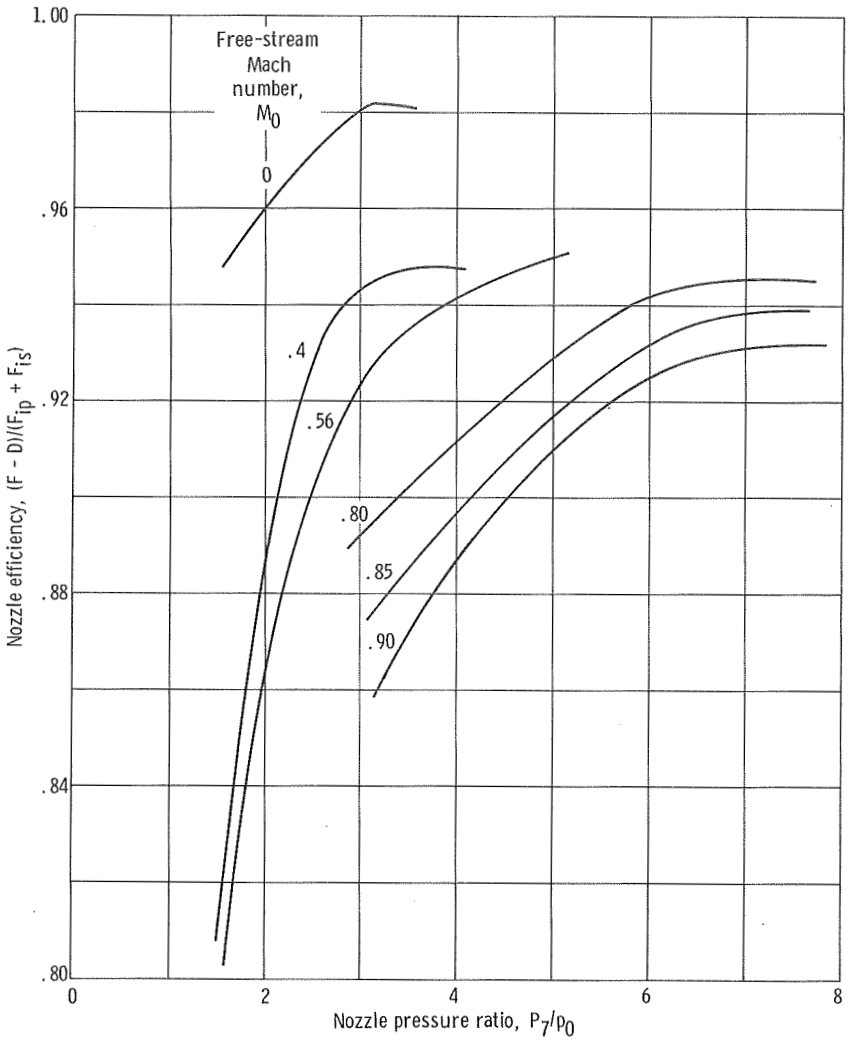

Figure 13. - Nozzle efficiency of nonafterburning configuration as function of nozzle pressure ratio for corrected secondary weight flow ratio of 0.04.

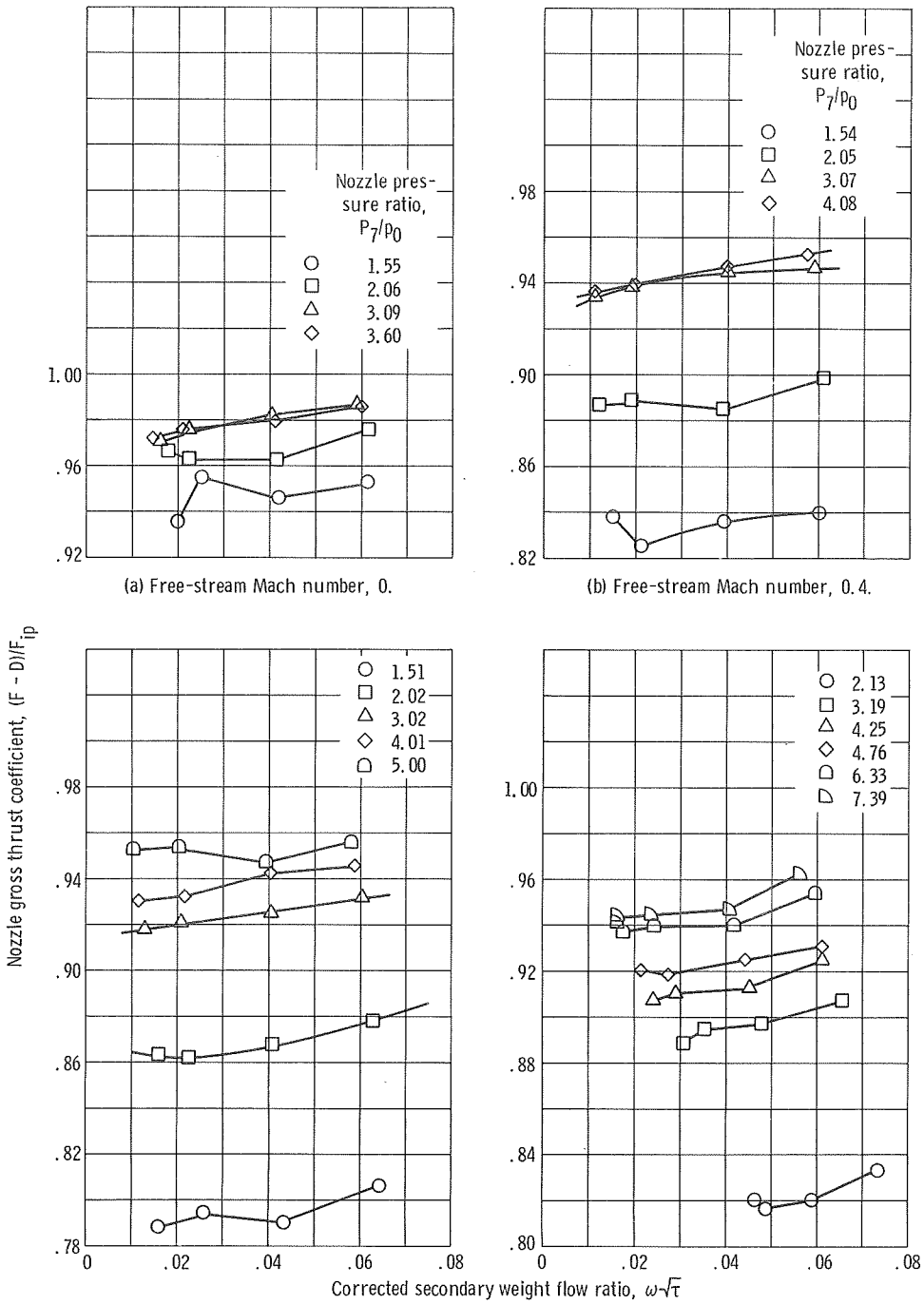

Figure 14. - Nozzle gross thrust coefficient as function of corrected secondary weight flow ratio for small primary.

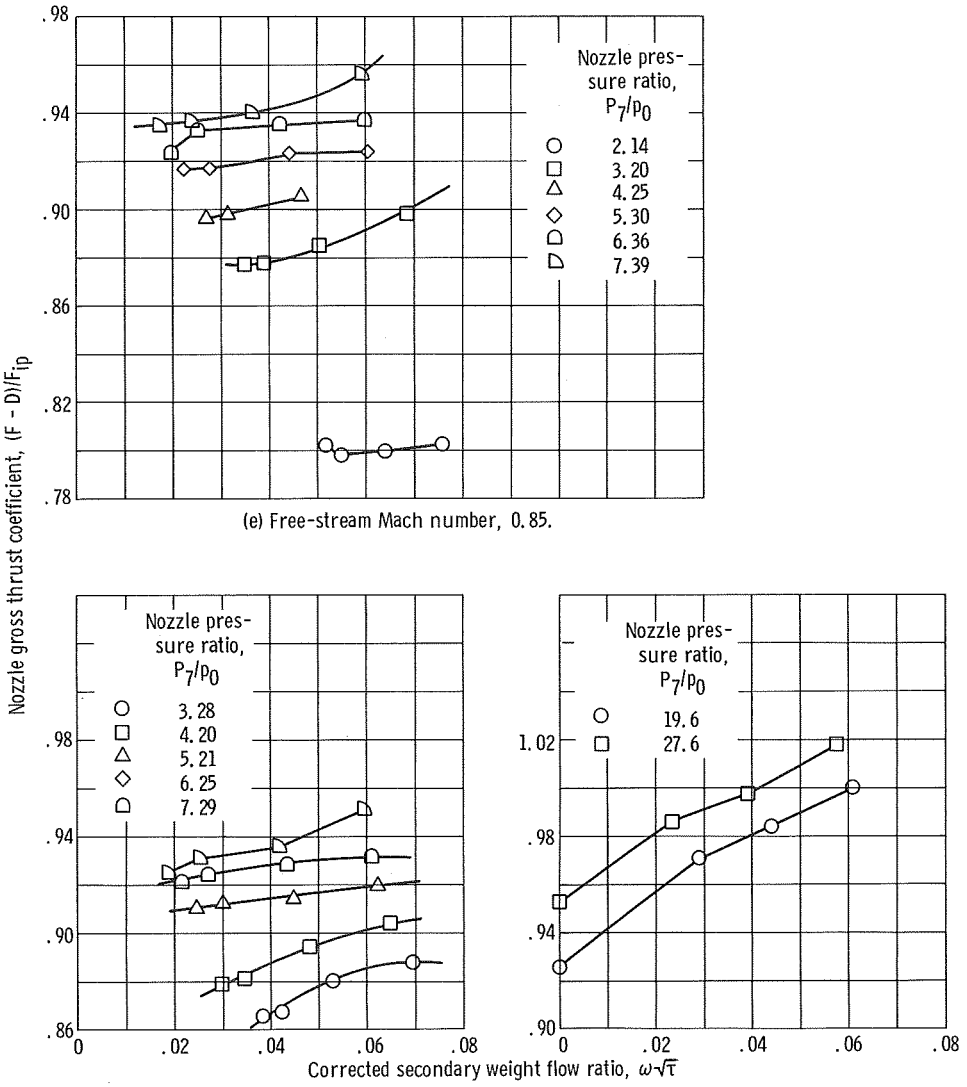

(e) Free-stream Mach number, 0.85.

(f) Free-stream Mach number, 0.9.

(g) Free-stream Mach number, 1.97.

Figure 14. - Concluded.

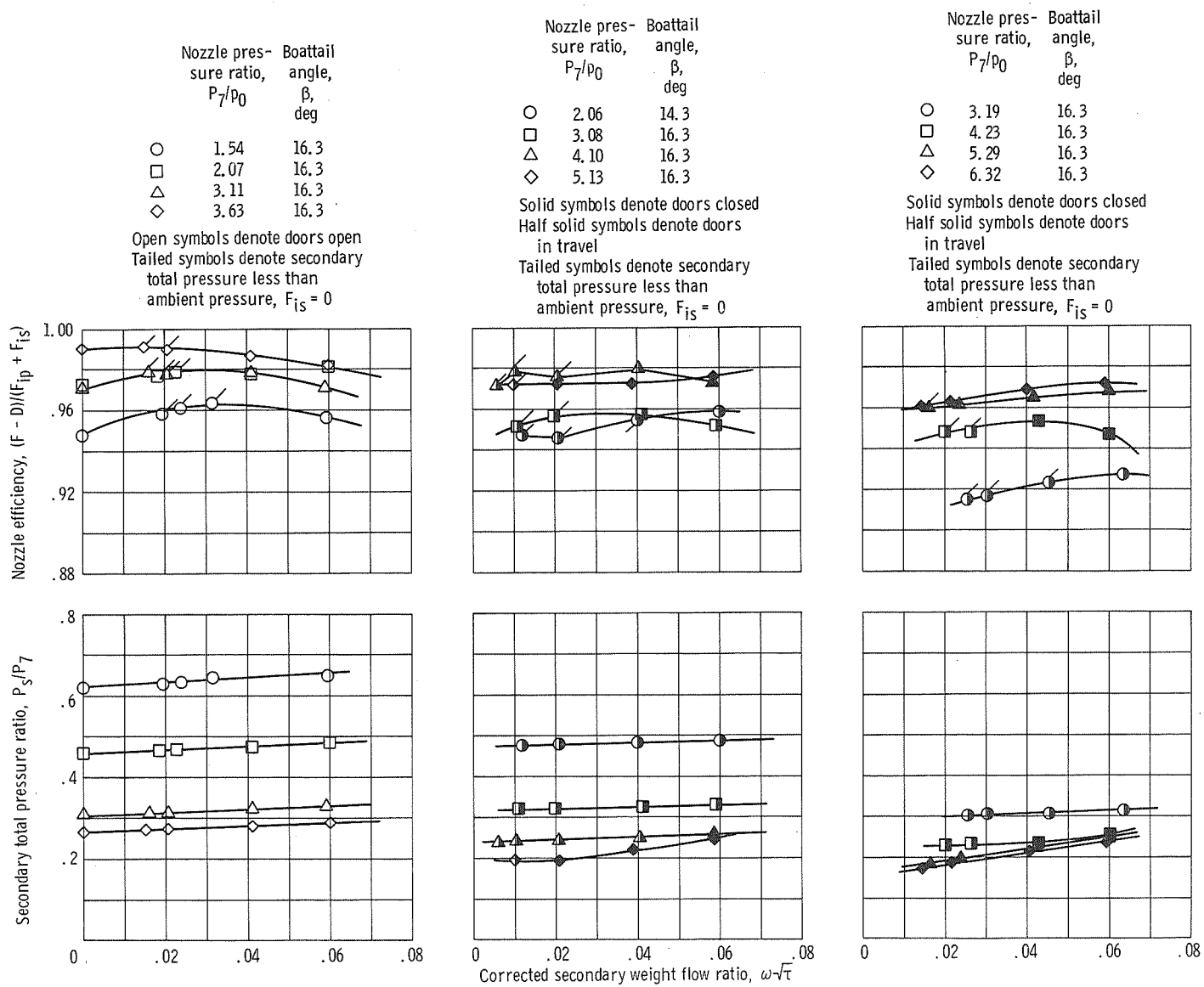

(a) Free-stream Mach number, 0.

(b) Free-stream Mach number, 0.4.

(c) Free-stream Mach number, 0.85.

Figure 15. - Nozzle efficiency and pumping characteristics as function of corrected secondary weight flow ratio for large primary.

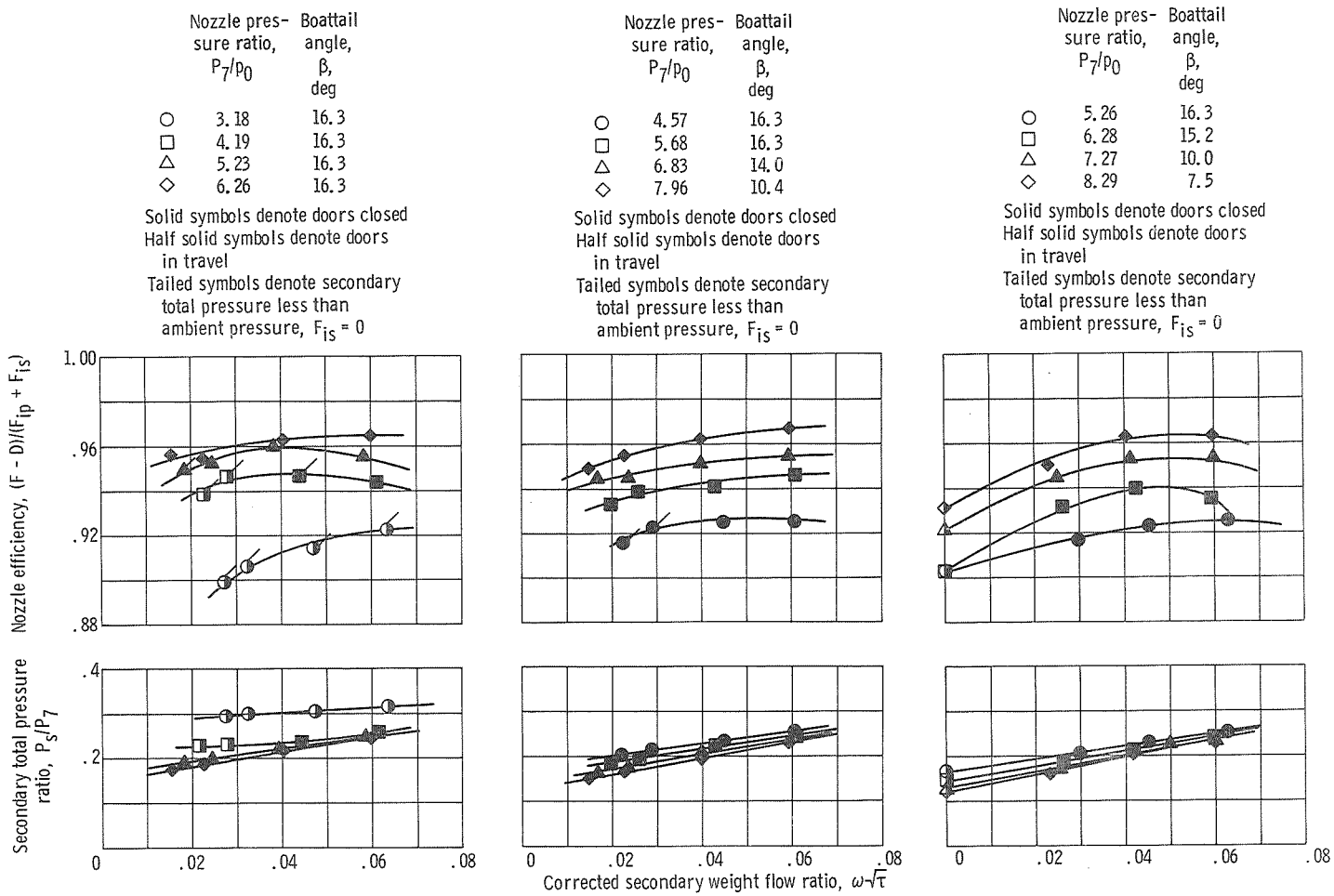

(d) Free-stream Mach number, 0.9.

(e) Free-stream Mach number, 1.0. Significant tunnel disturbances present.

(f) Free-stream Mach number, 1.09. Significant tunnel disturbances present.

Figure 15. - Continued.

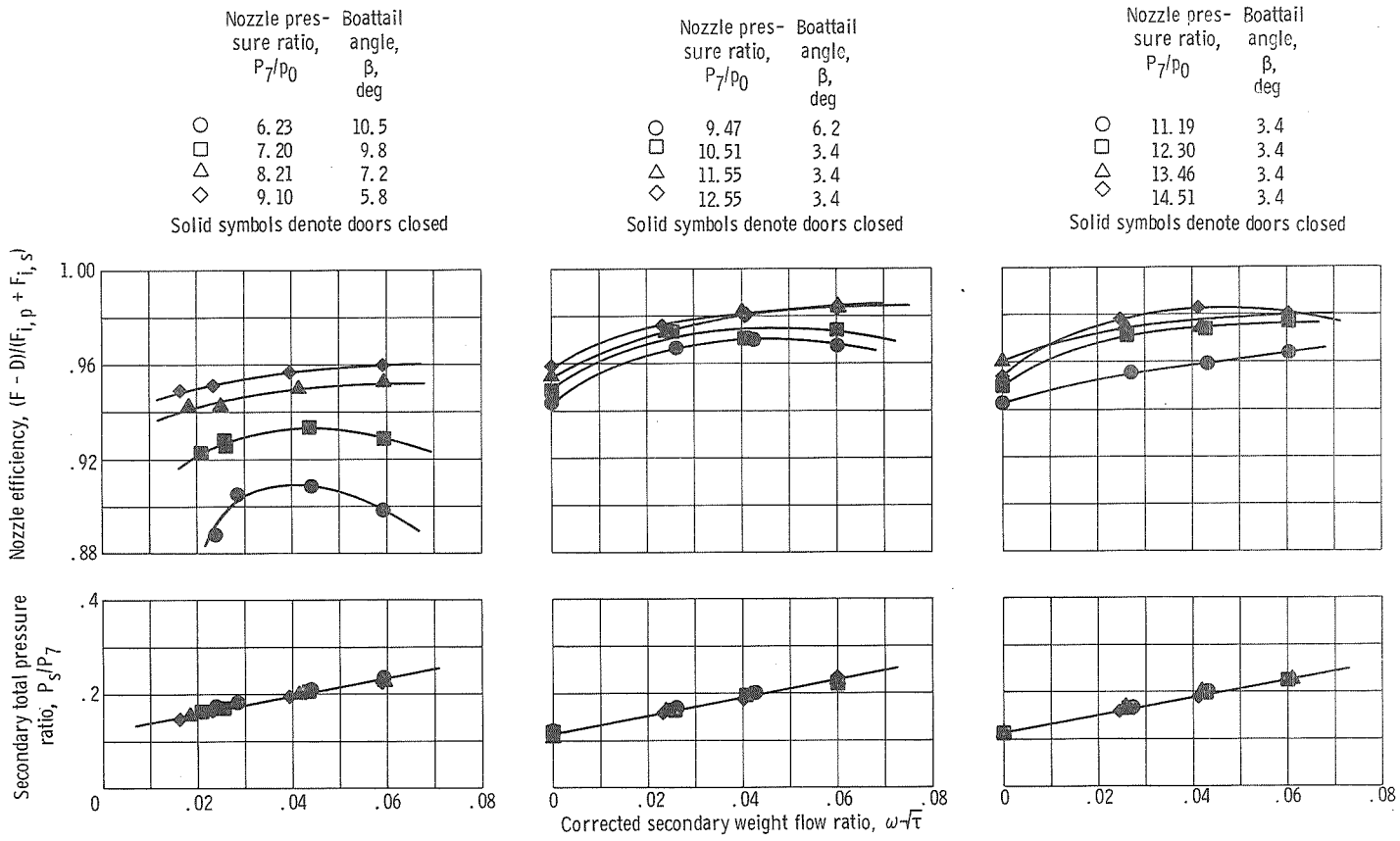

(g) Free-stream Mach number, 1.20.

(h) Free-stream Mach number, 1.47.

(i) Free-stream Mach number, 1.77.

Figure 15. - Concluded.

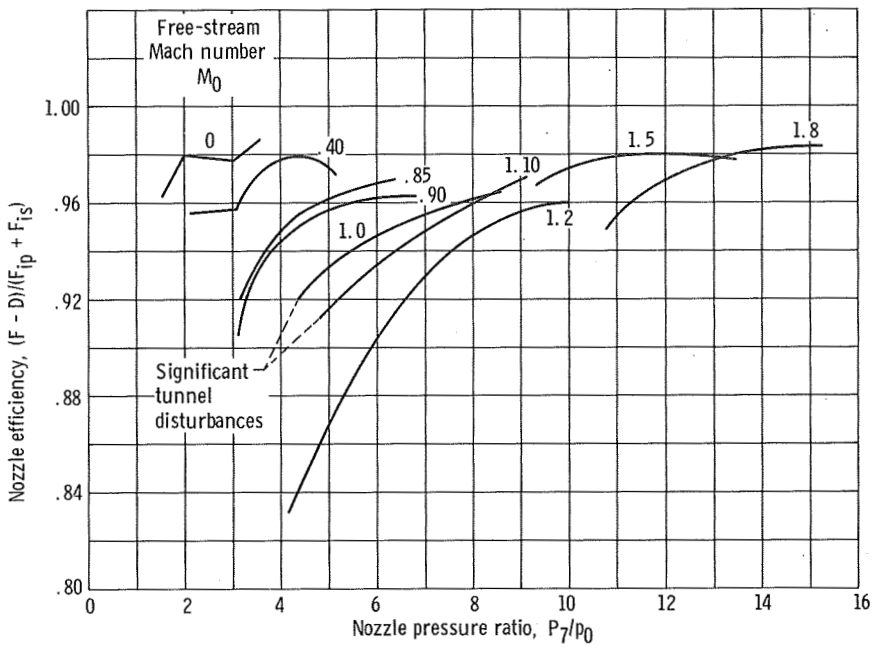

Figure 16. - Nozzle efficiency of afterburning configuration as function of nozzle pressure ratio for corrected secondary weight flow ratio of 0.04.

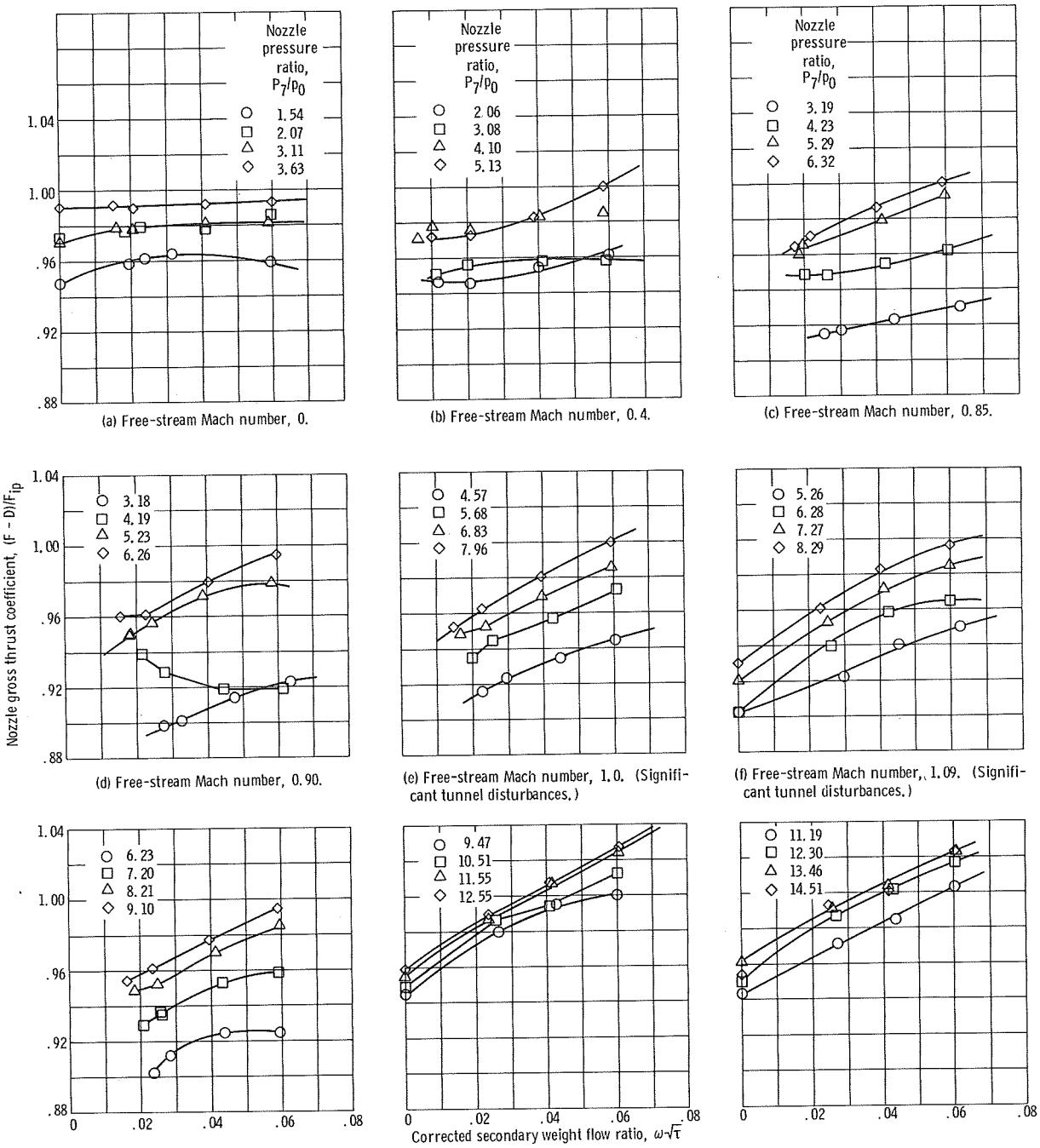

(a) Free-stream Mach number, 0.

(b) Free-stream Mach number, 0.4.

(c) Free-stream Mach number, 0.85.

(d) Free-stream Mach number, 0.90.

(e) Free-stream Mach number, 1.0. (Significant tunnel disturbances.)

(f) Free-stream Mach number, 1.09. (Significant tunnel disturbances.)

(g) Free-stream Mach number, 1.20.

(h) Free-stream Mach number, 1.47.

(i) Free-stream Mach number, 1.77.

Figure 17. - Nozzle gross thrust coefficient as function of corrected secondary weight flow ratio for large primary.

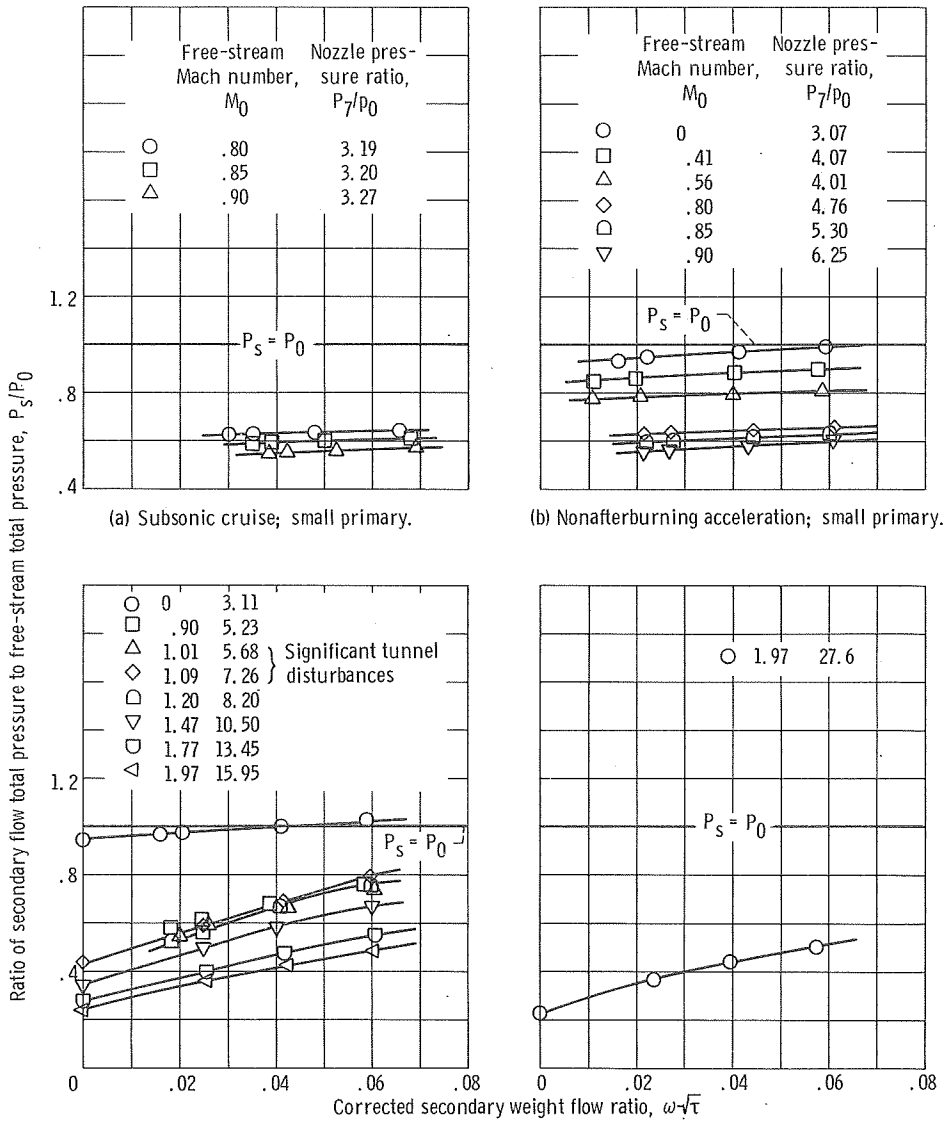

(a) Subsonic cruise; small primary.

(b) Nonafterburning acceleration; small primary.

(c) Afterburning acceleration; large primary.

(d) Supersonic cruise; small primary.

Figure 18. - Secondary flow pressure recovery requirement for various free-stream Mach numbers.

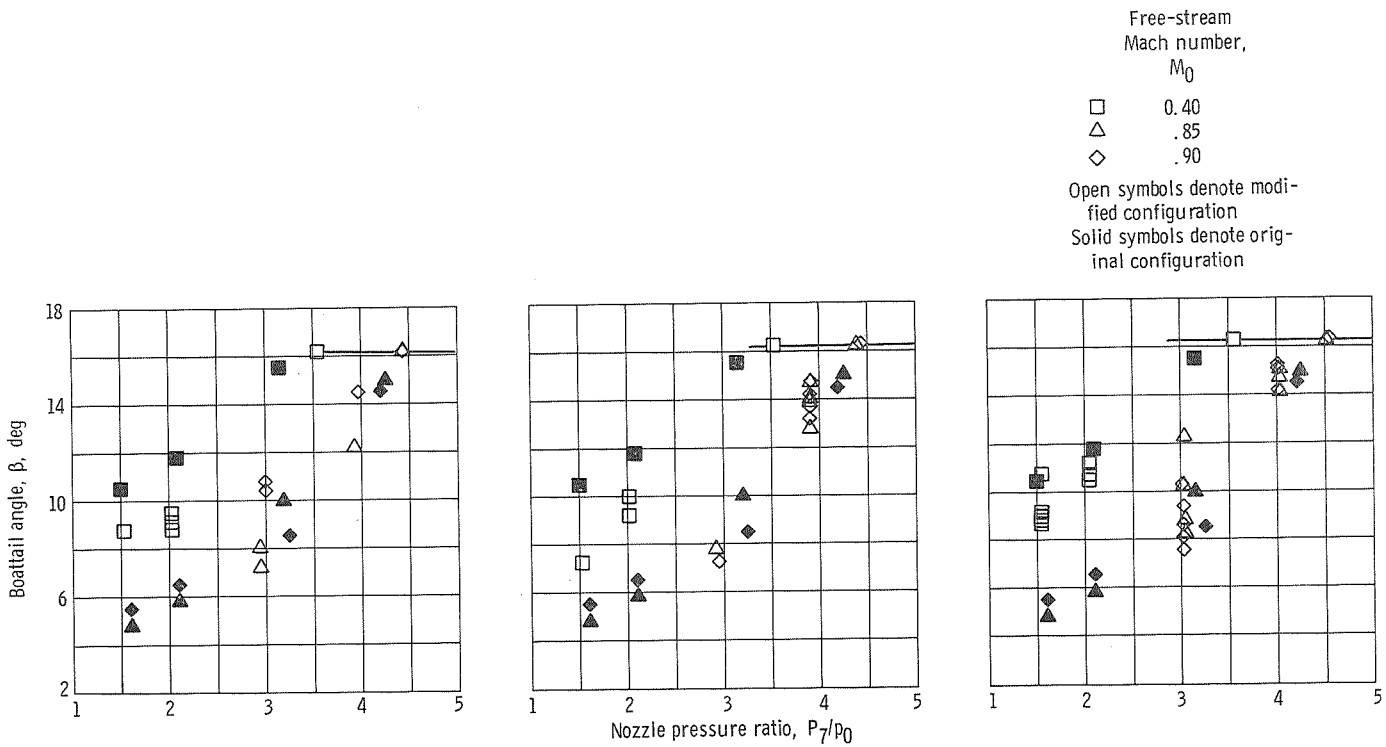

(a) Configuration 1.

(b) Configuration 2.

(c) Configuration 3.

Figure 19. - Variation of boattail angle with nozzle pressure ratio for modified nonafterburning configurations.

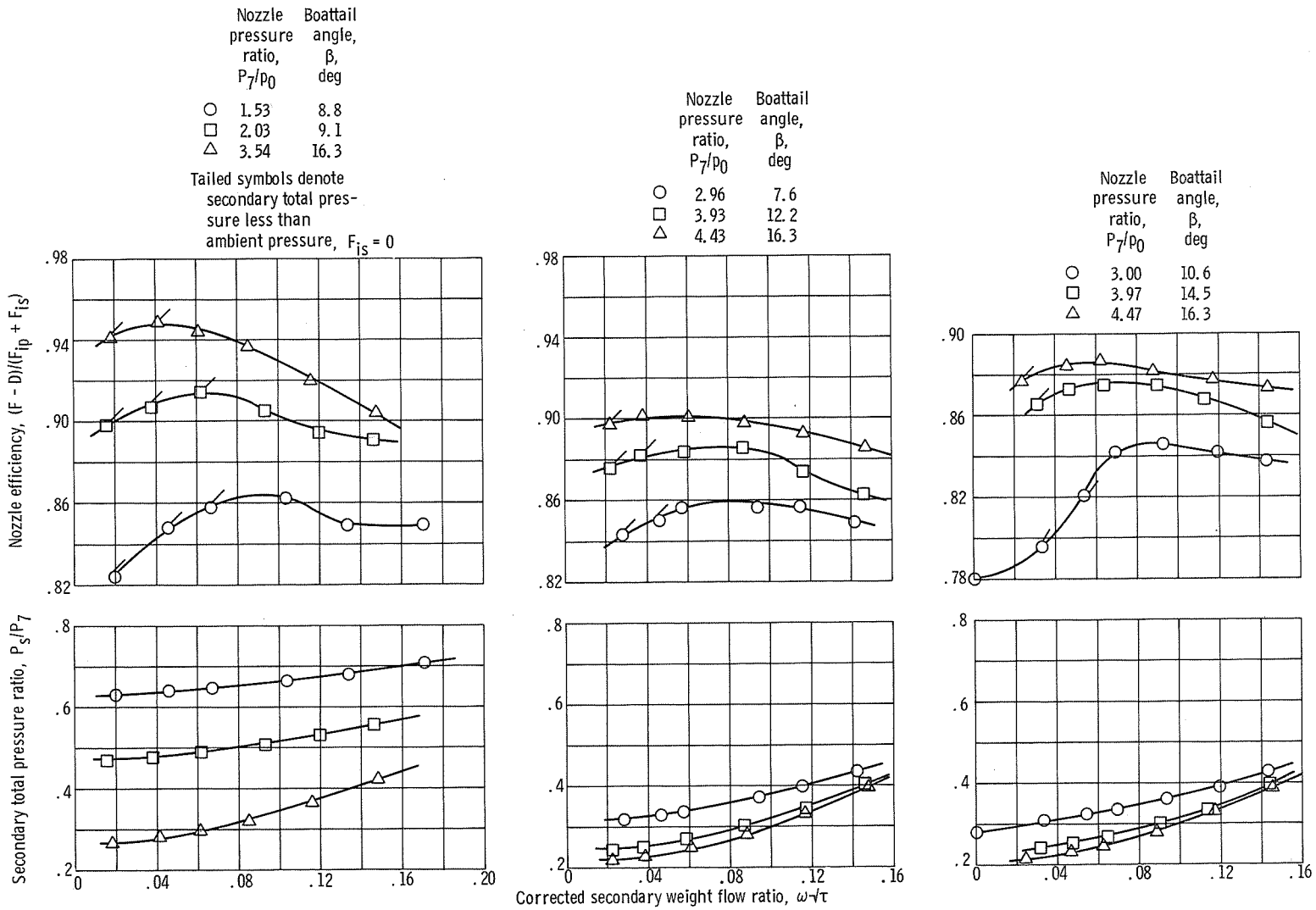

(a) Free-stream Mach number, 0.40.

(b) Free-stream Mach number, 0.85.

(c) Free-stream Mach number, 0.9.

Figure 20. - Nozzle efficiency and pumping characteristics as function of corrected secondary weight flow ratio for modified nonafterburning configuration 1. Doors fully open.

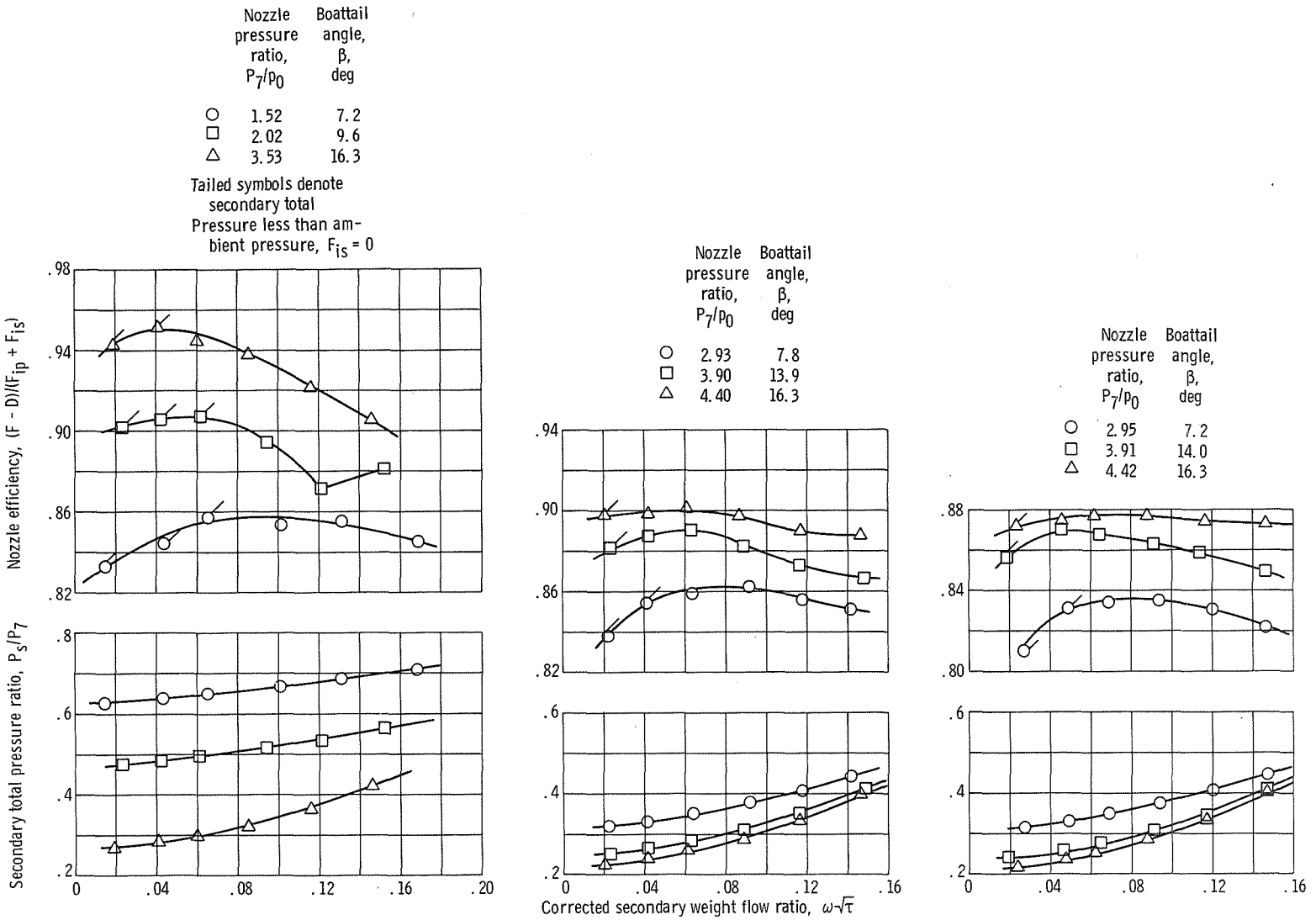

(a) Free-stream Mach number, 0.40.

(b) Free-stream Mach number, 0.85.

(c) Free-stream Mach number, 0.90.

Figure 21. - Nozzle efficiency and pumping characteristics as function of corrected secondary weight flow ratio for modified nonafterburning configuration 2. Doors fully open.

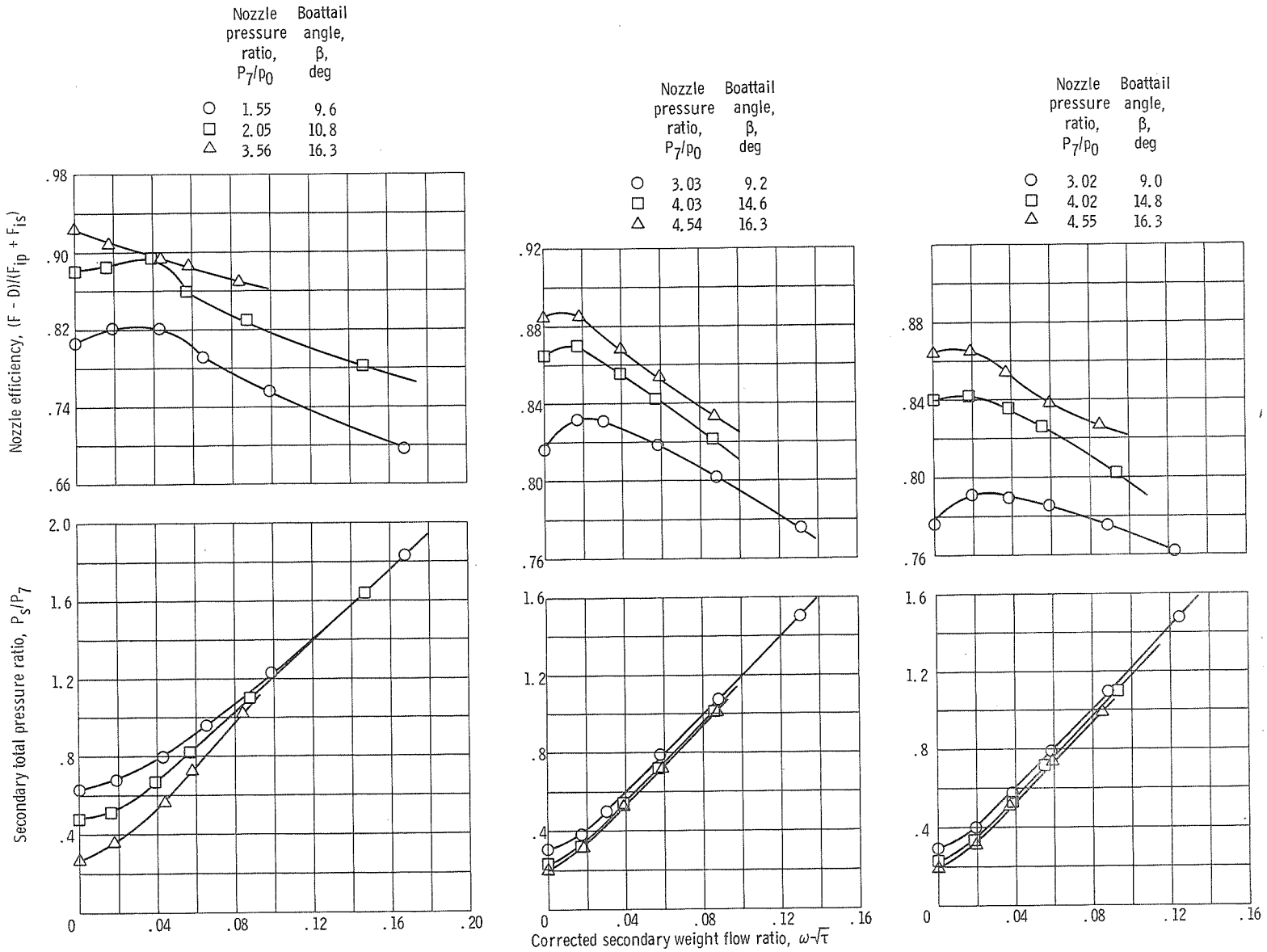

(a) Free-stream Mach number, 0.4.

(b) Free-stream Mach number, 0.85.

(c) Free-stream Mach number, 0.9.

Figure 22. - Nozzle efficiency and pumping characteristics as function of corrected secondary weight flow ratio for modified nonafterburning configuration 3. Doors fully open.

NASA-Langley, 1970 — 28 E-5536

NATIONAL AERONAUTICS AND SPACE ADMINISTRATION
WASHINGTON, D. C. 20546

OFFICIAL BUSINESS

FIRST CLASS MAIL

POSTAGE AND FEES PAID
NATIONAL AERONAUTICS AND
SPACE ADMINISTRATION

POSTMASTER: If Undeliverable (Section 158 Postal Manual) Do Not Return

"The aeronautical and space activities of the United States shall be conducted so as to contribute . . . to the expansion of human knowledge of phenomena in the atmosphere and space. The Administration shall provide for the widest practicable and appropriate dissemination of information concerning its activities and the results thereof."

— NATIONAL AERONAUTICS AND SPACE ACT OF 1958

NASA SCIENTIFIC AND TECHNICAL PUBLICATIONS

TECHNICAL REPORTS: Scientific and technical information considered important, complete, and a lasting contribution to existing knowledge.

TECHNICAL NOTES: Information less broad in scope but nevertheless of importance as a contribution to existing knowledge.

TECHNICAL MEMORANDUMS: Information receiving limited distribution because of preliminary data, security classification, or other reasons.

CONTRACTOR REPORTS: Scientific and technical information generated under a NASA contract or grant and considered an important contribution to existing knowledge.

TECHNICAL TRANSLATIONS: Information published in a foreign language considered to merit NASA distribution in English.

SPECIAL PUBLICATIONS: Information derived from or of value to NASA activities. Publications include conference proceedings, monographs, data compilations, handbooks, sourcebooks, and special bibliographies.

TECHNOLOGY UTILIZATION PUBLICATIONS: Information on technology used by NASA that may be of particular interest in commercial and other non-aerospace applications. Publications include Tech Briefs, Technology Utilization Reports and Notes, and Technology Surveys.

Details on the availability of these publications may be obtained from:

SCIENTIFIC AND TECHNICAL INFORMATION DIVISION

NATIONAL AERONAUTICS AND SPACE ADMINISTRATION

Washington, D.C. 20546